Chapter 4

Flow Modeling of Trickle Beds

Everything should be made as simple as possible, but not simpler.

Albert Einstein

INTRODUCTION

Conventional approaches for the analysis of trickle bed reactors are discussed in previous two chapters. Gross hydrodynamic characteristics of trickle bed reactors and different correlations for estimating key design parameters are summarized in Chapter 2. The interaction of downward flow of gas and liquid phases with closely packed solid particles leads to different flow regimes in trickle bed reactors. The classification of these flow regimes, their key characteristics, and influence on other important design parameters are also discussed in Chapter 2. The flow regime information is used for estimation of design parameters in the classical reaction engineering analysis for simulation of overall reactor performance as discussed in Chapter 3. The basic methodology discussed in these two previous chapters may not, however, be sufficient to establish quantitative relationship between reactor hardware/operating protocols and reactor performance, particularly at different scales of operation. The primary reason for this is these types of models do not adequately account for interaction of the hydrodynamics of the multiphase systems involved with various transport and kinetic processes occurring on different scales (from molecular scale to tens of meters). Such interactions over a wide range of scales cause severe difficulties in developing and solving predictive models to simulate reactor performance. It is often difficult to develop a single model to describe the complete reactor performance for a complex system such as a trickle bed reactor. Therefore, it is necessary to develop multilayer or multiscale models, which comprise of multiple models, each simulating processes occurring at different scales with different objectives and level of complexity. These models communicate the information with each other to provide adequately accurate estimation of the overall reactor performance. Such an approach for reactor engineering of trickle bed reactors is described here.

Trickle Bed Reactors. DOI: 10.1016/B978-0-444-52738-7.10001-4

Development of a trickle bed reactor design involves several steps such as:

- design or selection of a catalyst (composition, support, particle size/shape, surface area, porosity, etc.)
- development of rate equations and evaluation of kinetic parameters (understanding key chemical reactions, estimating intrinsic rate constants and activation energies, influence of catalyst conditioning, deactivation kinetics, etc.)
- evaluation of interphase and intraparticle (diffusion in porous catalysts; single component and multicomponent) mass transfer parameters under conditions of different flow regimes
- evaluation of key hydrodynamic characteristics (wettability, packing density, pressure drop, gas and liquid holdup, etc.)
- evaluation of scale-up/scale-down-related aspects (maldistribution, channeling, heat transfer, hotspots, residence time distribution (RTD), etc.)
- fine tuning scale-up and design of large-scale reactor (distributors, inlet–outlet nozzles, any other internals, location of temperature sensors, etc.)

The first four steps can be executed using the methods discussed in previous two chapters. These steps will lead to a preliminary design of a trickle bed reactor. Converting this preliminary design to a level that will be applicable at different scales of operation requires execution of the last two steps. Conventionally, the scale-up issues (the last two steps) are addressed based on the experience and engineering judgment of design engineers. In this chapter, an attempt will be made to develop a comprehensive multiscale analysis methodology based on a sound scientific approach. A brief introduction to the elementary processes occurring on different scales in a trickle bed reactor is given in Chapter 1 (see Figs. 5 and 6 and associated discussion). The processes occurring within the catalyst pores and on active catalyst sites can be quantitatively analyzed using the methods discussed in Chapter 3. In this chapter, methods for analysis of processes occurring on scales of individual catalyst particles, group of particles (meso-scale processes), and catalyst bed (macroscale processes) in a trickle bed reactor are discussed. When integrated with the issues discussed in Chapters 2 and 3, these methods will provide means to implement steps listed above, involved in the development of trickle bed reactor design. Some other practical aspects of reactor engineering of trickle beds are discussed in Chapter 5.

In this chapter, key issues like characterization of individual catalyst particle, packing density, and packed bed of such particles are discussed. Different possible arrangements of catalyst particles in the bed and their influence on other parameters are discussed in the next section. Mathematical ways of constructing and quantitatively characterizing packed beds are briefly discussed. Single-phase flow through group of particles is then discussed in the section *Single-Phase Flow Through Packed Bed*. It provides basic information on drag exerted by a fluid on particles, flow structures in packed bed, local heat

and mass transfer parameters, etc. Gas–liquid flow through packed bed is discussed under the section *Gas–Liquid Flow Through Packed Bed*. Computational models to simulate gas–liquid flow through large packed beds of catalyst particles are discussed in this section. Meso-scale models which may provide better insight into wetting and interaction of liquid phase with solid particles are also briefly discussed. Applications of these flow models for simulating RTD and chemical reactions in trickle bed reactors are then discussed. An attempt is made to provide a general framework and guidelines for using different computational models for constructing as complete picture of the large-scale trickle bed reactor as possible.

CHARACTERIZATION OF PACKED BEDS

The main objective in designing trickle bed reactors is to improve effective contact of gas and liquid phase reactants with the active catalyst sites; provide adequate residence time and allow dissipation of liberated heat of reactions without causing any hotspots and catalyst deactivation. Usually, the following factors are considered while designing a packed bed for trickle flow operation:

Pressure drop: Operating cost of trickle bed reactors is directly related to pressure drop across the bed and is crucially dependent on the structure of the bed and operating flow rates. It is possible to manipulate the bed structure (particle characteristics and packing characteristics) to reduce pressure drop without jeopardizing the overall performance of the reactor. Maintaining a stable pressure drop is also essential for smooth operation of the reactor for prolonged period of time.

Specific surface area: Effective contacting of reactants with active catalyst site and heat/mass transfer efficiency are determined by available specific surface area as one of the factors.

Residence time distribution/mixing: It is essential to understand the relationship between bed structure and resulting RTD in order to achieve the desired RTD by manipulating the bed structure. Catalyst particle size, shape, and surface characteristics (to manipulate wetting) influence RTD. Maldistribution and channeling of the liquid or gas flow, which adversely influence the overall reactor performance, depend on bed structure and method of packing. Liquid and gas phase axial and radial mixing is also influenced by local bed structure and associated meso-scale flow processes. The existence of dead zones (stagnant pockets) in the reactor reduces effective utilization of packed catalyst. The bed structure needs to be designed to minimize if not eliminate such dead zones.

Liquid holdup: Higher liquid holdup is usually beneficial for efficient mass transfer and higher reaction rates and therefore the bed structure needs to be manipulated to achieve higher liquid holdup.

Heat and mass transfer: Particle shape, size, and local arrangements influence local flow structure and therefore local heat and mass transfer rates.

These local transport rates become important when the reaction is mass transfer limiting or temperature sensitive.

It is obvious that these different aspects may impose conflicting demands on bed structure. For example, a structure that provides higher heat and mass transfer rates usually leads to higher pressure drop. It is therefore essential to consider these different aspects and evolve a compromise solution appropriate for a specific case under consideration.

The physical nature of the catalyst surface on which chemical transformations occur is quite crucial. Active catalytic material consisting of metals/metal oxides or their complexes is deposited on the surface of a carrier material (alumina, silica, or specially designed zeolites or metallic surface). In most cases, catalyst particles are porous and the active material is impregnated on the surface of internal pores. Chemical reactions occur on catalyst sites available on these micro-pores within the catalyst particles. In some cases, to avoid diffusional resistances, catalyst is impregnated on outer surface (or shell) instead of impregnating inside the entire particles. This is called eggshell-type catalyst particles. If reaction is highly exothermic, non-porous catalyst particles are used where reaction occurs only on the external surface of the particles. Sometimes, catalyst is coated on a structured support instead of particles. Apart from the distribution of chemically active sites, physical nature of the catalyst comprising size, shape of particle, density, surface area per unit volume, surface characteristics (roughness wetting), heat capacity, thermal conductivity, attrition resistance, and strength to compression load are also important. The effective catalyst life is dependent on possibility of leaching, thermal deactivation, or sintering, etc. Historically, spherical and cylindrical-shaped porous catalyst particles are widely used. In recent years, several new shapes of catalyst particles have been proposed for industrial applications (see Fig. 1 of Chapter 1 and discussion in the section *Particle Characteristics* of Chapter 5).

After selection of a particular type of catalyst, next important task is to design the nature of packed bed and packing structure. Most widely used practice is to pack the catalyst particles randomly inside the bed as shown in Fig. 1a. However, several other ways of realizing semi-structured and structured packing of catalyst particles have also been proposed (Irandoust & Anderson, 1988; Mewes, Loser, & Millies, 1999; Van Hasselt, Lindenbergh, Calis, Sie, & Van Den Bleek, 1997). A schematic of structured packing arrangement is shown in Fig. 1b. A brief discussion on characteristics of random and structured beds is provided in the following sections.

Randomly Packed Bed

Randomly packed beds are used in majority of industrially operated trickle bed reactors because of their simplicity in construction and loading procedure. Randomly packed catalyst particles are generally spherical, cylindrical,

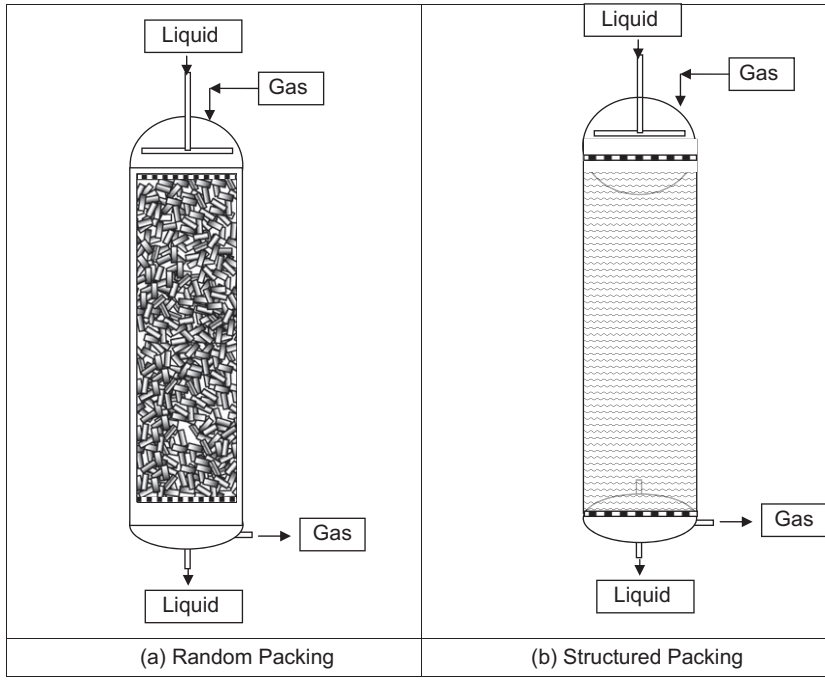

FIGURE 1 A schematic of random and structured packing. (a) Random packing; (b) structured packing.

extrudates, trilobes, or quadrilobes. Selection of particle size and shape is often based on the desired pressure drop in the system as well as other transport characteristics like external and intraparticle mass and heat transfer. Attrition and durability (stiffness) of particles are also important parameters for selecting the catalysts. Catalyst attrition may occur during loading of catalysts which may lead to a higher pressure drop and loss of catalyst. There are several methods for realizing such a random packing in practice as described by Al-Dahhan, Wu, and Dudukovic (1995). When particles are packed randomly in a cylinder, the characteristic of packing depends significantly on the ratio of particle size to the bed diameter and on the shape of particles.

Numerous studies on porosity distribution in randomly packed beds are available (Donohue & Wensrich, 2008; Mantle, Sederman, & Gladden, 2001; Spedding & Spencer, 1995; Stephenson & Stewart, 1986). These experimental and computational studies have shown that the bed porosity is higher near the vicinity of the reactor wall and it fluctuates significantly in the near wall region (of width of about 4−5 particle diameters). Mueller (1991) has proposed a correlation for radial variation of axially averaged porosity as a function of column diameter, particle diameter, and average porosity. This

correlation (Eq. (1)) represents the available experimental data with a reasonable accuracy:

$$\varepsilon(r) = \varepsilon_B + (1 - \varepsilon_B) J_o(ar^*) e^{-br}.$$

where,

$$a = 8.243 - \frac{12.98}{(D/d_p - 3.156)} \quad \text{for } 2.61 \le D/d_p \le 13.0$$

$$a = 7.383 - \frac{2.932}{(D/d_p - 9.864)} \quad \text{for } 13.0 \le D/d_p$$

$$b = 0.304 - \frac{0.724}{D/d_P}$$

$$r^* = r/D \quad \text{and} \quad J_o \text{ is zero-th order Bessel function} \tag{1}$$

The predicted radial variation of bed porosity for 11.4 cm column diameter for two particle sizes is shown in Fig. 2 as an illustration.

Jiang, Khadilkar, Al-Dahhan, and Dudukovic (2001) have shown that the porosity variation in axial direction (at any radial location) is close to the Gaussian distribution. The value of standard deviation of such a distribution decreases with increase in the ratio of column diameter to particle diameter and eventually approaches to zero for very small (compared to column diameter) particles. The porosity distribution within the randomly packed bed may thus be represented by imposing random fluctuations (following the Gaussian distribution) over the axially averaged porosity estimated by Mueller's correlation (see,

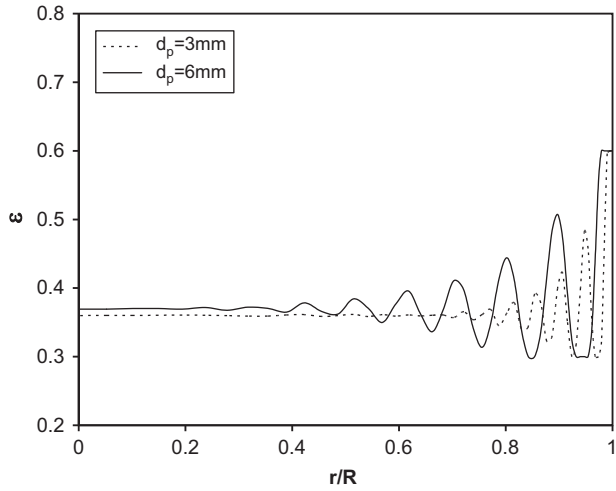

FIGURE 2 Variation of bed porosity along radial direction using Mueller (1991) correlation for column diameter of 11.4 cm (Gunjalet al., 2005). System: $D = 0.114$ m, 3 mm or 6 mm glass beads.

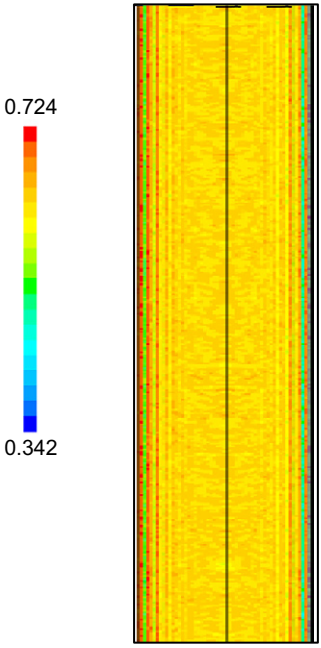

FIGURE 3 Contours of radial and axial variation of solid holdup implemented in computational model (Gunjal et al., 2005). System: $D = 0.194$ m, 6 mm glass beads.

for example, Gunjal, Kashid, Ranade, & Chaudhari, 2005). A sample of random solid phase distribution as a result of implementation of porosity distribution generated by the above method is shown in Fig. 3. Such randomly distributed bed porosity may give more realistic results than assuming mean porosity all over the bed. It must be noted that the porosity distribution observed in a packed bed will be obviously dependent on the scale of scrutiny. It has been experimentally shown that on the scale of a cluster of particles, porosity has the Gaussian distribution (Jiang, Khadilkar, Al-Dahhan, & Dudukovic, 2000) while at a much smaller scale porosity has a bi-modal distribution (Jiang et al., 2001). This relationship between porosity distribution and scale of scrutiny (scale of interest) should be kept in mind while generating randomly distributed porosity within a bed.

Most of the information available in open literature is, however, restricted to spherical particles. Comparison of a radial variation of porosity with trilobe and spherical particles is shown in Fig. 4. It can be seen that fluctuations in porosity with trilobes are less than those observed with the spherical particles. In the absence of adequate information on porosity distribution for catalyst particles of different shapes, discrete element methodology may be used to quantify characteristics of the packed beds (Donohue & Wensrich, 2008). These computational models simulate random packing of the bed and provide a useful framework to quantitatively understand the influence of particle size and shape on characteristics of the randomly packed beds. A sample of such simulated bed packing is shown in Fig. 5 (Donohue & Wensrich, 2008).

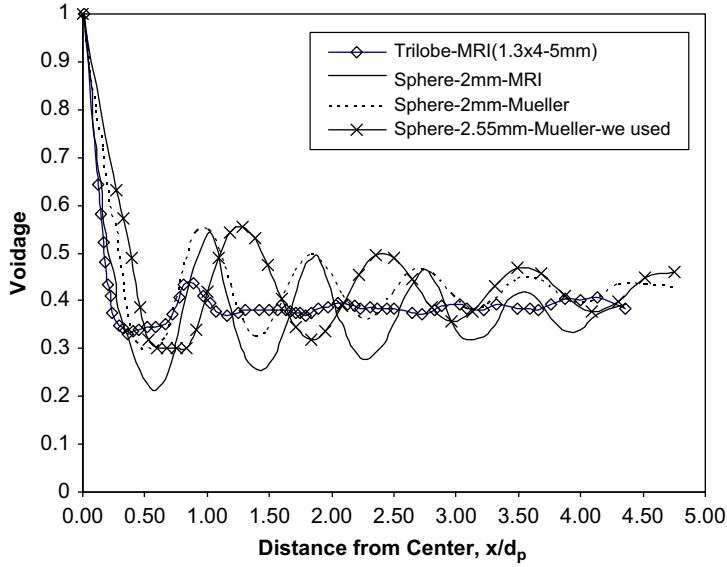

FIGURE 4 Variation of porosity for different catalyst sizes and shapes (Gunjal & Ranade, 2007). System: $D = 0.0224$ m, $\varepsilon = 0.5$.

Structured Bed

In order to avoid likely build up of higher pressure drop associated with the random packing, attempts have been made to use semi-structured or fully structured packed beds for trickle bed reactors. The ideas about the structured packing mainly originated from their successful application in distillation columns. High surface area per unit volume, lower pressure drop, and relatively straightforward scale-up are some of the key advantages of the structured packing. Therefore, structured packing may be preferred over the random unstructured packing for processes requiring higher mass transfer rates and lower pressure drop. However, structured packing is expensive compared to the conventional unstructured packing and often needs additional support mechanisms for installation inside the reactors. Several types of structured packing as listed below may be used in the trickle bed reactors:

- Gauze packing
- Corrugated sheet packing
- Mesh-type packing
- Monoliths/honeycomb (Irandoust & Anderson, 1988)
- Three layer packing (Van Hasselt et al., 1997)

Structured packing can be incorporated in reactors by several ways; for example, arranged in continuous stacked form with or without offset, structured packing incorporated in a pipe, and arranged on the sieve plates. Structured

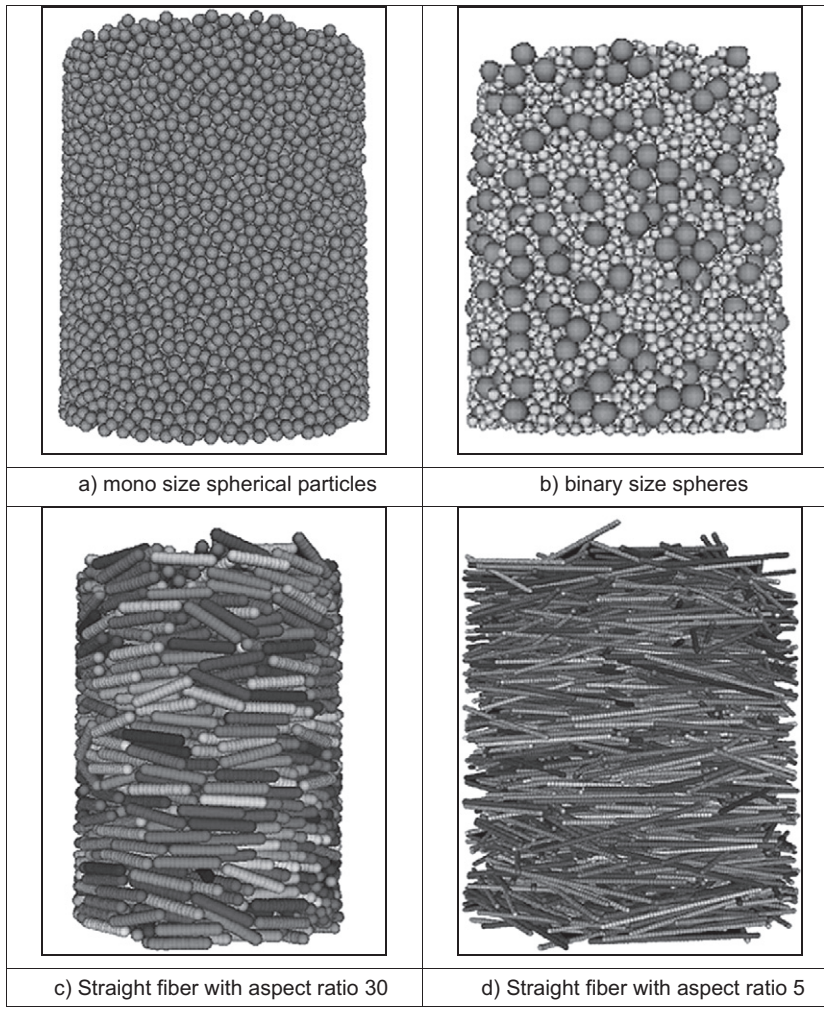

FIGURE 5 Simulated packed beds with particles of different shapes (Donohue & Wensrich, 2008). (a) Mono size spherical particles; (b) binary size spheres; (c) straight fiber with aspect ratio 30; (d) straight fiber with aspect ratio 5.

packing is characterized in terms of characteristic scale of repeat unit, surface area per unit volume, and void fraction. Some examples of the structured packing are shown in Fig. 6.

It is important to accurately quantify characteristics of the packed bed (characteristic length scales and porosity distribution) to facilitate better understanding of the flow behavior of gas and liquid phases. The available information and models for obtaining insight into flow through trickle beds are discussed in the following.

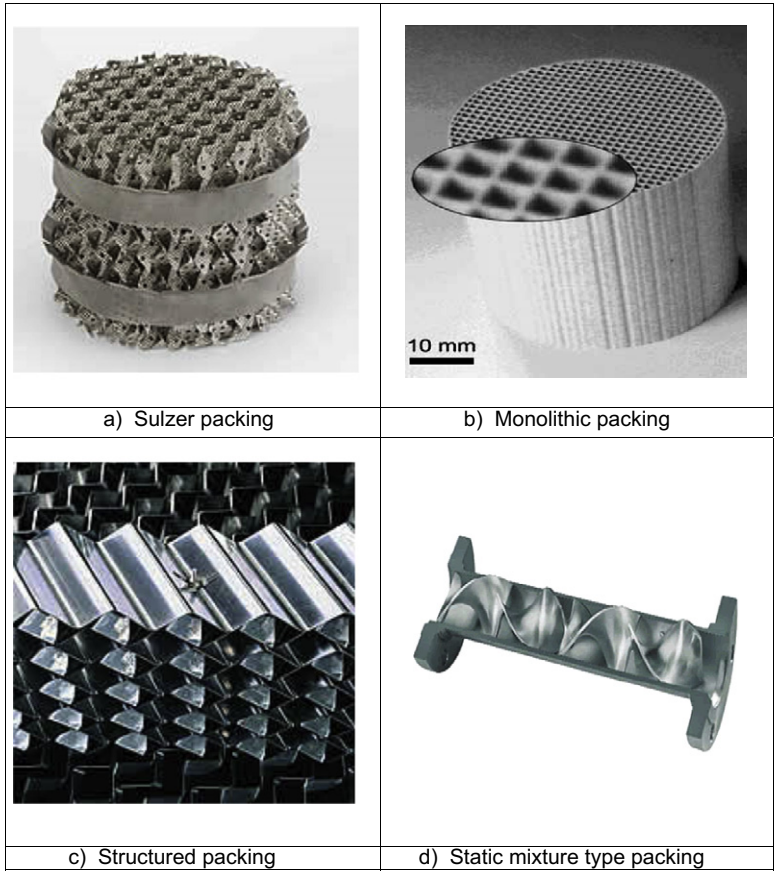

FIGURE 6 Different types of structured packing used in trickle bed reactors (http://www.sulzerchemtech.com/). (a) Sulzer packing; (b) monolithic packing; (c) structured packing; (d) static mixture-type packing.

SINGLE-PHASE FLOW THROUGH PACKED BED

In trickle bed reactors, gas and liquid phases flow cocurrently downward through the packed bed of catalyst particles. Multiphase flow through complex interstitial geometry formed by bed particles controls mixing and other transport processes occurring in trickle bed reactors. It is important to gain insight into the local flow behavior and transport processes occurring in the packed bed to be able to tailor, monitor, and optimize its performance. Considering the complexities of the multiphase flow through packed bed, it is necessary to first develop a clear understanding of the single-phase flow inside the bed before proceeding to the analysis of multiphase flow behavior. Some of the key aspects of single-phase flow through packed bed and the various approaches of

computational modeling have been discussed in this part to create a platform for further discussion on gas−liquid flow through packed beds.

Besides its importance for understanding the multiphase flow behavior, single-phase flow through the packed bed is also encountered in a variety of applications ranging from flow through capillary column of a gas chromatograph to flow through pebbles in the riverbed. Single-phase flow occurs via void region present in the bed consisting of interconnected pores and tortuous path. In trickle bed reactors, the catalyst bed is usually filled with porous catalyst particles. The transport inside such porous particles is mainly controlled by diffusional processes and therefore is not significantly influenced by flow through voids formed due to packing of particles. However, the mass and heat transfer external to the catalyst particles and axial as well as radial mixing can be significantly affected by the changes in the flow behavior of the gas and liquid phases through the bed. Flow through voids of packed bed has been extensively studied using experimental as well as computational models. Prevailing regimes of single-phase flow through packed beds depending on the gas and liquid velocities are briefly discussed in Chapter 2. Key aspects of different regimes of single-phase flow through packed beds are highlighted in the following.

Sangani and Acrivos (1982) and SØrensen and Stewart (1974) have analyzed the flow through unit cells with particles arranged in simple cubical (SC) and face centered cubic (FCC) patterns several years ago. They have reported predicted drag force exerted on particles at different values of porosity. Their studies, however, were limited to the Stokes flow regime ($Re \rightarrow 0$). The Stokes flow regime exists at very low particle the Reynolds number (~<0.1) where average drag force on particles is independent of Reynolds number. Considering the usual operating ranges of packed beds, it is, however, essential to understand the flow characteristics in the inertial flow regime (particle Reynolds number > 10). Only recently some attempts of analyzing inertial flow in packed beds have been made.

Durst, Haas, and Interthal (1987) simulated laminar flow through unit cells and compared simulated pressure drop with experimental data. Maier, Kroll, Kutovsky, Davis, and Bernard (1998) have carried out lattice Boltzmann simulations of single-phase flow through FCC and random packing arrangement of particles. They presented some comparisons of simulated velocity distribution with their experimental results. Their study was restricted to low Reynolds numbers ($Re = 0.5-29$). Tobis (2000) has used unit cell approach for simulating turbulent flow in a packed bed. Hill, Koch, and Ladd (2001) have carried out the lattice Boltzmann simulations of flow through FCC, SC, and random arrangement of particles. Detailed analysis of drag force variation with solid volume fraction and packing arrangement was discussed. Freund et al. (2003) have carried out the lattice Boltzmann simulations of flow in a packed bed reactor of a low aspect ratio (~5). They studied relative contributions of skin and form drag in overall pressure drop. However, in these studies, detailed

analysis of flow structure in a packed bed and its influence on rates of other transport processes was not presented. Recently, Magnico (2003) has carried out simulations for a unit cell and for small tube-to-sphere diameter ratio over the range of Reynolds numbers (from 7 to 200). He demonstrated the influence of flow structures on mass transfer with the help of the Lagrangian particle tracking.

Extensive experimental data of flow through packed beds are now available. Mantle et al. (2001), Sederman and Gladden (2001), and Sederman, Johns, Bramley, Alexander, and Gladden (1997) have experimentally characterized flow in packed beds and have reported measured distributions of axial and transverse velocities in the interstitial space. The axial velocity distribution showed a sharp peak and was asymmetrical. The transverse velocity distribution showed exponential decay in both positive and negative directions. Experimental data reported by Maier et al. (1998) also showed similar trends of velocity distributions. Suekane, Yokouchi, and Hirai (2003) have carried out detailed measurements of flow through voids of simple packed bed using magnetic resonance imaging (MRI) and have provided detailed quantitative data on velocity distributions. They also reported details of inertial flow structures for different Reynolds numbers. It is more effective to use such comprehensive data sets to validate computational models and use the validated models for further investigations. Several attempts have been made recently to develop computational models for simulating the flow behavior (flow structures, velocity field) in packed beds (see, for example, Calis, Nijenhuis, Paikert, Dautzenberg, & van den Bleek, 2001; Dixon & Nijemeisland, 2001; Freund et al., 2003; Logtenberg, Nijemeisland, & Dixon, 1999; Tobis, 2000; Zeiser et al., 2002).

Apart from such detailed studies of meso-scale flow, computational models have also been used to quantify macroscopic flow characteristics such as maldistribution or channeling in packed beds (mixing and RTDs). In such cases, the entire bed is modeled as a porous medium. The local porosity values are specified by averaging over a control volume, significantly larger than the particle size. Before describing a sample of results and key aspects of single-phase flow through packed beds, modeling approaches used for such studies are briefly reviewed in the following.

Modeling Approaches

Flow through a packed bed can be modeled using various approaches depending on the objectives and intended use. These approaches are schematically shown in Fig. 7.

In all of these approaches mass and momentum balance equations are solved to simulate detailed flow characteristics around particles/bed of particles. In the first approach (A), entire packed bed consisting of a number of particles (either arranged in a regular fashion or in a random fashion) is

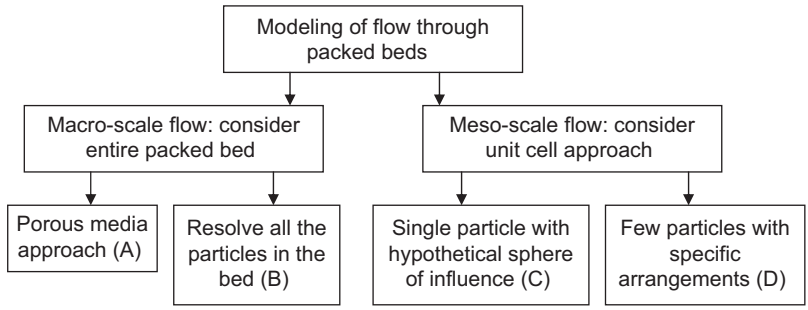

FIGURE 7 Modeling approaches.

considered. Porous media approach (A), however, does not provide information about the local flow and transport occurring within the bed. It provides the macroscopic information. Other three approaches (B−D) can provide local information (on particle scale) and are discussed here. Calis et al. (2001), Logtenberg et al. (1999), and Nijemeisland and Dixon (2001) among others have used the approach (B). Computational constraints often limit the size of the bed and the number of particles considered in such simulations. Therefore, often the "unit cell approaches" (C, D) are used.

As shown in Fig. 7, there are two sub-types in the unit cell approach. In the first type (C), each particle is assumed to have a hypothetical sphere of influence around it (see Dhole, Chhabra, & Eswaran, 2004 and references cited therein). Flow is solved around a particle placed in a hypothetical sphere of influence (size of which depends on porosity of the bed). This approach, however, ignores differences caused by different particle arrangements and therefore was not considered here. In the second type of unit cell approach (D), a unit "periodic" cell composing of few particles is considered. The packed bed is represented by periodically repeating the unit cell in all the three directions. This approach is being used traditionally to analyze transport processes in packed beds (see, for example, Martin, McCabe, & Monrad, 1951; SØrensen & Stewart, 1974). Different packing arrangements of particles like SC, rhombohedral, and FCC or body centered cubic (BCC) can be considered for representing the packed bed. This approach is illustrated here.

The approach of unit cells, where packed bed of spheres is represented by geometrically periodic unit cells with different packing arrangements, is advantageous to understand flow structures in large packed beds. It is, however, essential to understand the possible implications of approximating a packed bed by periodic unit cells. It is well known that symmetry of a flow over a single sphere breaks when particle Reynolds number increases beyond 105 and unsteady flow occurs (Natarajan & Acrivos, 1993). The unit cell approach is not valid for cases where periodic symmetry of flow is absent despite the symmetric and periodic geometry. Fortunately, when particles are packed closely together in a regular fashion, the onset of symmetry breaking unsteady

flow is delayed considerably (Hill et al., 2001). The largest length scale characterizing the interstitial region of the regular arrays is smaller than particle diameter. Therefore, the Reynolds number characterizing the stability of the flow in the interstitial region can be up to approximately 2.5 times larger than the critical particle Reynolds number. Secondly, at larger solid volume fractions, the fluid is increasingly confined and hence stabilized by neighboring spheres. For a specific particle Reynolds number, viscous dissipation will be higher at higher solid volume fraction, and therefore more effective in damping velocity fluctuations. Considering this, the unit cell approach can be used to understand the influence of particle Reynolds number and packing arrangement on inertial flow structures in packed beds.

Model Equations and Boundary Conditions

For approaches (B), (C), and (D), classical single-phase flow equations with appropriate selection of solution domain and boundary conditions can be used. Laminar flow of an incompressible fluid through a packed bed of spheres can be simulated by solving the Navier−Stokes equations. The study of Seguin, Montillet, and Comiti (1998) and Seguin, Montillet, Comiti, and Huet (1998) indicated that the flow in packed bed exhibits a transition regime over a large range of particle Reynolds number and the turbulent flow regime may exist beyond $Re_p = 900$. Therefore, when particle Reynolds number exceeds 1000, the Reynolds-averaged Navier−Stokes equations (RANS) along with suitable turbulence model need to be used (see Ranade, 2002 for more discussion on modeling of turbulent flows). Reynolds-averaged Navier−Stokes equations for mass and momentum balance for incompressible Newtonian fluid are given by,

$$\frac{\partial u_i}{\partial x_i} = 0 \tag{2}$$

$$\frac{\partial u_i}{\partial t} + \frac{\partial \left(u_i u_j\right)}{\partial x_j} = -\frac{1}{\rho}\frac{\partial P}{\partial x_i} + \frac{\partial}{\partial x_j}\left[\left(\nu + \nu_t\right)\left(\frac{\partial u_i}{\partial x_j} + \frac{\partial u_j}{\partial x_i}\right)\right] \tag{3}$$

where, u_i is the mean velocity in the i direction, P is the pressure and ν_t is the turbulent kinematic viscosity. The turbulent kinematic viscosity, ν_t, needs to be estimated using an appropriate turbulence model. The two-equation standard $k-\varepsilon$ model of turbulence is one of the most widely used turbulence models and can be used as a starting point to simulate turbulent flow in packed beds. The governing equations of this model can be written as:

$$\nu_t = C_\mu \frac{k^2}{\varepsilon} \tag{4}$$

$$\frac{Dk}{Dt} = \frac{\partial}{\partial x_j}\left[\left(\nu + \frac{\nu_t}{\sigma_k}\right).\frac{\partial k}{\partial x_j}\right] + G - \varepsilon \quad G = \nu_t \frac{\partial u_i}{\partial x_j}\left(\frac{\partial u_i}{\partial x_j} + \frac{\partial u_j}{\partial x_i}\right) \tag{5}$$

$$\frac{\mathrm{D}\varepsilon}{\mathrm{D}t} = \frac{\partial}{\partial x_j}\left[\left(\nu + \frac{\nu_t}{\sigma_\varepsilon}\right).\frac{\partial \varepsilon}{\partial x_j}\right] + \frac{\varepsilon}{k}(C_{1\varepsilon}G - C_{2\varepsilon}\varepsilon) \tag{6}$$

The standard values of the parameters appearing in Eqs. (5) and (6) were used ($C_{1\varepsilon} = 1.44$, $C_{2\varepsilon} = 1.92$, $C_\mu = 0.09$, $\sigma_\kappa = 1.0$, and $\sigma_\varepsilon = 1.3$: from Launder & Spalding, 1974).

The energy conservation equation (without any source or sink) may be written as:

$$\frac{\partial(\rho h)}{\partial t} + \nabla\cdot(\rho u_i h) = (k + k_t)\nabla^2 T \tag{7}$$

where h is enthalpy, k is thermal conductivity, and k_t is turbulent thermal conductivity. First term in the right-hand side is of the effective conductive heat flux (molecular and turbulent). The turbulent thermal conductivity is given by,

$$k_t = \frac{C_p \mu_t}{Pr_t} \tag{8}$$

In order to model the unit cell as a representative piece of a packed bed, periodic boundary conditions need to be implemented at all the faces of the unit cell through which flow occurs. In such a translational periodic boundary condition, all the variables except pressure (and enthalpy or temperature) at periodic planes are set to be equal. For a desired particle Reynolds number, superficial velocity and mass flow rates were calculated based on the considered geometry. However, pressure is not periodic; instead the pressure drop is periodic. Because the value of pressure gradient is not known a priori, it must be iterated until the specified mass flow rate is achieved in the computational model. No slip boundary condition needs to be implemented on all the impermeable walls. For turbulent flow simulations, it may not be possible to resolve the steep gradients near walls without excessively increasing demands on computing resources. In such cases, a concept of "wall functions" is used (standard wall function of Launder & Spalding, 1974). Several extensions of the basic wall functions have been developed (see, for example, enhanced wall function by Jongen, 1992; Kader, 1993; Wolfstein, 1969; non-equilibrium wall function by Kim & Choudhury, 1995; generalized wall functions by Popovac & Hanjalic, 1997). For carrying out heat transfer simulations; if the interest is to simulate heat transfer coefficient, it may be necessary to resolve the steep gradients near the walls adequately. The heat transfer coefficient from solid wall to the fluid can then be calculated as;

$$q = hA(T_w - T_b) = -k_f\left(\frac{\partial T}{\partial n}\right)_{\text{wall}} \tag{9}$$

where, n is the normal coordinate normal to the wall and k_f is the thermal conductivity of the fluid phase. The subscripts w and b denote wall and bulk, respectively.

Approaches (B), (C), and (D) are more suitable as learning models or as supportive tools for validation of data collected experimentally. This may also reduce use of empirical parameters while modeling actual reactor. For example, local particle to fluid heat transfer coefficient can be calculated with high accuracy using the above approach for known flow rates and particle type. The results obtained based on the assumption of periodic array need to be interpreted and connected to the flow in large bed of particles. This relationship is not straightforward and requires characterization of different possible packing arrangements in the large bed. In the absence of such characterization, the approach (A) is more suitable in practice for simulating flow through large packed beds. In this approach, instead of actually simulating the packing geometry inside the column and solving governing equation of single-phase flow in the void spaces inside the reactor, bed of randomly packed particles is considered as a continuous porous medium with predefined porosity distribution. This assumes that definition of a volume fraction of solids (over a suitable control volume) is meaningful. Continuity and momentum balance equations are derived using appropriate averaging. Additional source terms representing resistance offered by the porous medium (randomly packed bed) are included in the momentum equations. More details of this approach and governing equations may be found elsewhere (Ranade, 2002). Unlike the other three modeling approaches, the approach (A) can be applied to industrial-scale packed beds. However, in the formulation of the averaged governing equations, some semi-empirical interaction and closure terms are involved. Hence, supportive experiments and models as well as learning models (direct simulation or periodic assumption approach) are required. Some of the results obtained with the approaches discussed here are described in the following section.

Flow Through an Array of Particles

Different types of flow patterns were observed during single-phase flow through periodic array of particles depending upon the flow rates, properties of fluids, and loading of solid. Mantle et al. (2001), Sederman and Gladden (2001), and Sederman et al. (1997) have experimentally characterized flow in packed beds and have reported measured distributions of axial and transverse velocities in interstitial space. They also reported details of inertial flow structures for different Reynolds numbers. Gunjal, Chaudhari, and Ranade (2005a) have validated their computational model using the data of Suekane et al. (2003). Some of these results are reproduced here for providing glimpses of key characteristics of flow through array of particles.

Simple Cubic Arrangement of Spheres

It is important to ensure that predicted results are not influenced by numerical parameters like discretization schemes and grid size when computational models described in the previous section are used for flow simulations. Higher

order discretization schemes are recommended. It is also useful to carry out numerical experiments to quantify influence of grid size, distribution, and discretization schemes on predicted results. Comparison of results predicted by Gunjal et al. (2005a) with the experimental data of Suekane et al. (2003) is shown in Fig. 8.

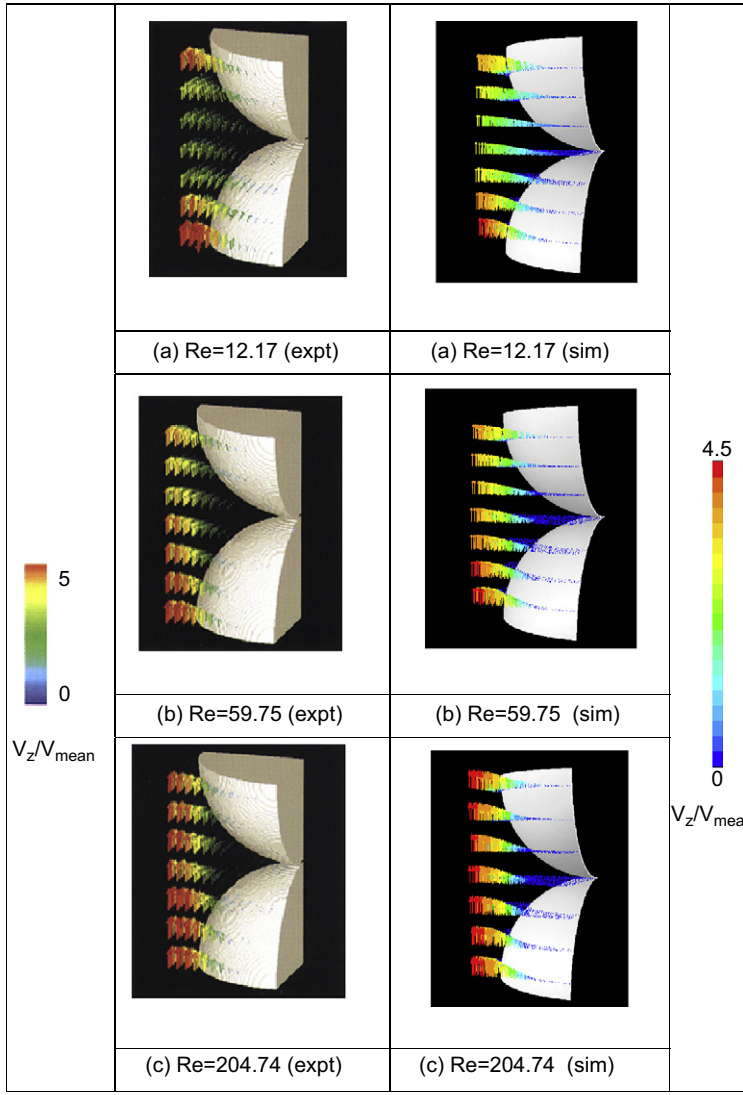

FIGURE 8 Comparison of simulated results of z-velocity (axial velocity) with experimental data at different particle Reynolds numbers (Gunjal et al., 2005a). (a) Re = 12.17; (b) $Re = 59.75$; (c) $Re = 204.74$.

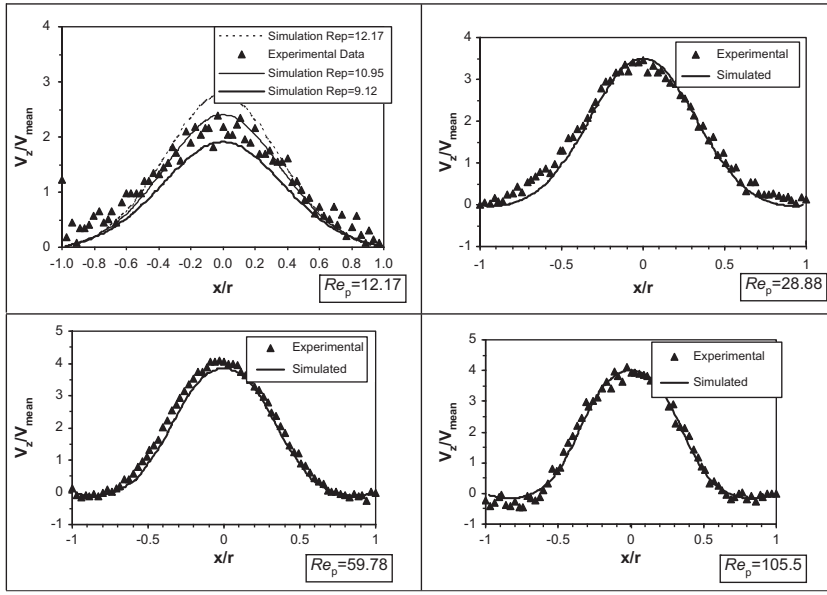

FIGURE 9 Comparison of simulated z-velocity (axial velocity) distribution with experimental data at various Reynolds numbers. Velocity measured at z midplane along x-axis at $y = 0.0015$ (Gunjal et al., 2005a).

It can be seen that variation of axial velocity was captured reasonably well in the simulated results. At highest Reynolds number ($Re_p = 204.74$), where inertial forces are dominant, jet-like flow behavior was observed in the experimental flow fields (see Fig. 8c). Similar, dominant velocity stream through the center of the solution domain was also observed in the simulation. Quantitative comparison of the simulated and the measured z-components of the velocity is shown in Fig. 9. Simulated results showed good agreement with the experimental data except at the lowest value of Reynolds number (12.17). It is interesting to note that experimental results also show highest scatter at this particle Reynolds number. Possible difficulties in maintaining a steady flow at a very low flow rate may be one of the reasons for such scatter. It can be seen (from Fig. 9) that the reported experimental data for the lowest Reynolds number (12.17) lie in between the results predicted for $Re_p = 9.12$ (25% less than 12.17) and 10.95 (10% less than 12.17).

Simulated results of flow field were also found to capture experimentally observed flow structures quite well (see Fig. 10 for $Re_p = 59.78$ and Fig. 11 for $Re_p = 204.74$). It is noteworthy that at higher Reynolds number (204.74), the observed and simulated flows at plane C are qualitatively different than those observed at lower Reynolds number (59.78). Further simulations at higher particle Reynolds number show that the normalized velocity profiles are almost independent of Reynolds number unlike in the laminar flow regime (where

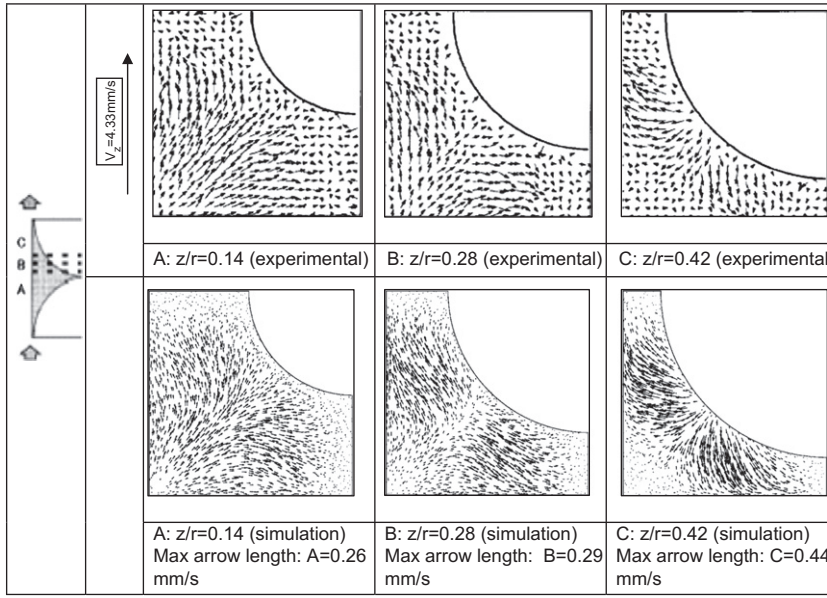

FIGURE 10 Comparison of the simulated flow field at three horizontal planes with experimental data at $Re_p = 59.78$ (Gunjal et al., 2005a).

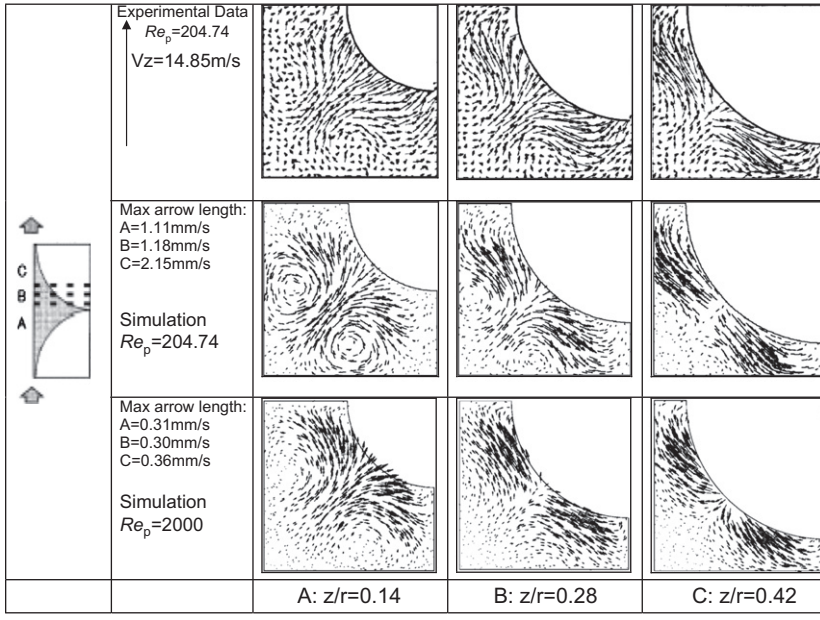

FIGURE 11 Comparison of the simulated flow field with experimental data at three horizontal planes ($Re_p = 204.74$ and 2000).

maximum in profiles of normalized axial velocities increases with increasing Reynolds number). The maximum value of normalized velocity in turbulent regime is closer to that obtained with the lowest Reynolds number considered in the laminar regime ($Re_p = 12.17$). Velocity profiles for the turbulence cases are much flatter than those obtained for the laminar regime. The region of negative velocities near the wall was found to be larger in turbulent flow regime compared to the laminar regime. Inertial flow structures were similar to those observed at particle Reynolds number of 204.74. Knowledge of such detailed flow structure within void spaces will have significant implications for the estimation of heat and mass transfer parameters. For example, simulated results of Gunjal et al. (2005a) indicate substantial difference in the predicted Nusselt numbers for the FCC arrangement and SC arrangement of spheres. Influence of particle arrangement on resulting flow structures and velocity distribution is briefly discussed in the following section.

Influence of Packing Arrangement of Spheres

In order to understand the influence of packing arrangement of particles in unit cell, results of Gunjal et al. (2005a) are discussed here. These simulations were carried out for different particle arrangements: namely one-dimensional rhombohedral ($\varepsilon = 0.4547$), three-dimensional rhombohedral ($\varepsilon = 0.2595$), and FCC ($\varepsilon = 0.302$) arrangements. Simulations were carried out at different particle Reynolds numbers in laminar flow regime ($Re_p = 12.17-204.74$) and in turbulent flow regime ($Re_p = 1000, 2000$).

Simulated results for one-dimensional rhombohedral arrangement at different particle Reynolds number are shown in Fig. 12. It can be seen that flow at lower Reynolds number (12.17 and 59.78) is qualitatively different than that at higher Reynolds numbers (204.74 and 2000). At higher Reynolds number, wake behind the spheres divides the high velocity stream in two parts at periodic planes (see two groups of red vectors in Fig. 12c and d). Profiles of predicted normalized z-component of the velocity on periodic plane at $x = 0.0015$ are shown in Fig. 13. At lower Reynolds number ($Re_p = 12.17$), flow profile is bell shaped with maximum velocity of about twice the mean velocity ($V_{max} = 2V_m$). With increase in Reynolds number, flow profile is flattened and wake behind the solid body starts affecting the flow profiles. At $Re_p = 2000$, splitting of high velocity stream into two parts is obvious from the shown velocity profiles (Fig. 13). Comparison of Figs. 13 and 9 clearly demonstrates the influence of packing arrangement on the flow in interstitial spaces. It can be seen from Fig. 9 that for SC arrangement the ratio of the z-component of velocity to the mean velocity is 2.5 for the lowest Reynolds number and increases up to 4 with increase in Reynolds number. For the rhombohedral arrangement, the value of this ratio is always below 2 (Fig. 13). Unlike SC, the flow encounters obstruction and changes the direction for rhombohedral arrangement of particles.

The predicted drag coefficients for FCC and SC geometry with solid volume fraction equal to 0.5 are shown in Fig. 14. It is quite clear that

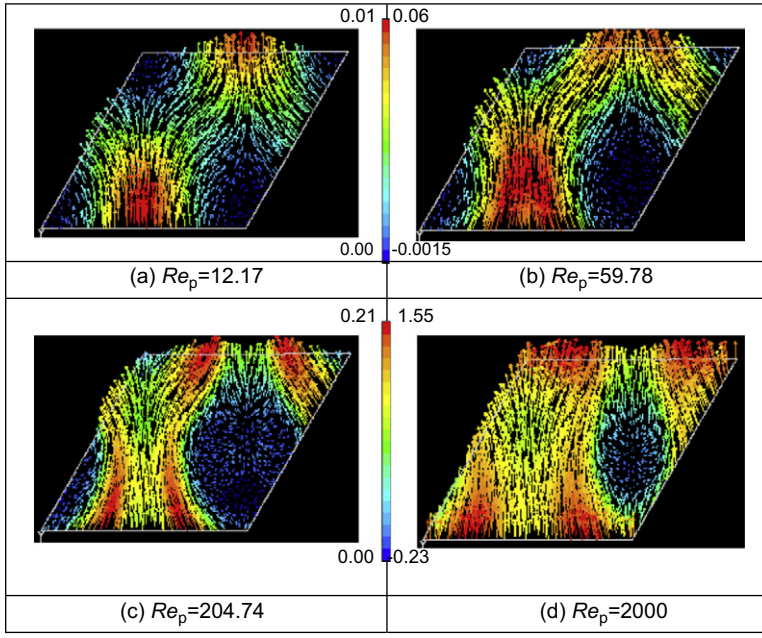

FIGURE 12 Velocity vectors and z-velocity (axial velocity) distribution in rhombohedral cell at various particle Reynolds numbers (Gunjal et al., 2005a). (a) $Re_p = 12.17$; (b) $Re_p = 59.78$; (c) $Re_p = 204.74$; (d) $Re_p = 2000$.

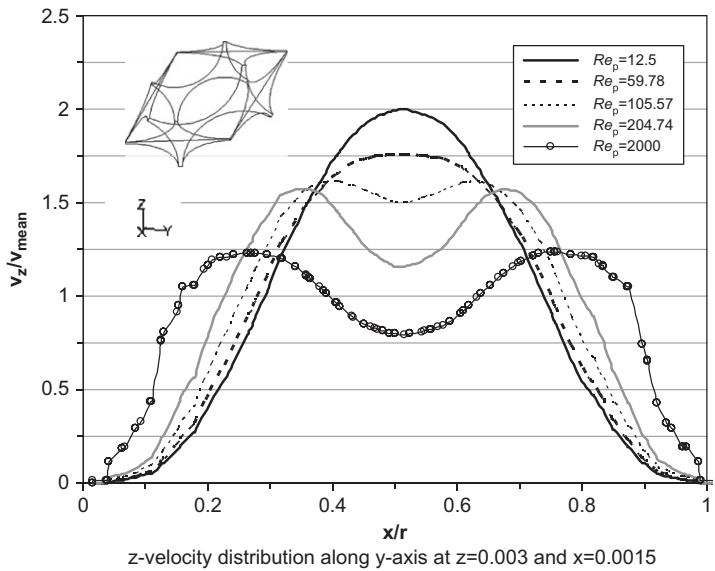

FIGURE 13 Velocity vectors and z-velocity (axial velocity) distribution in rhombohedral cell at various particle Reynolds numbers (Gunjal et al., 2005a).

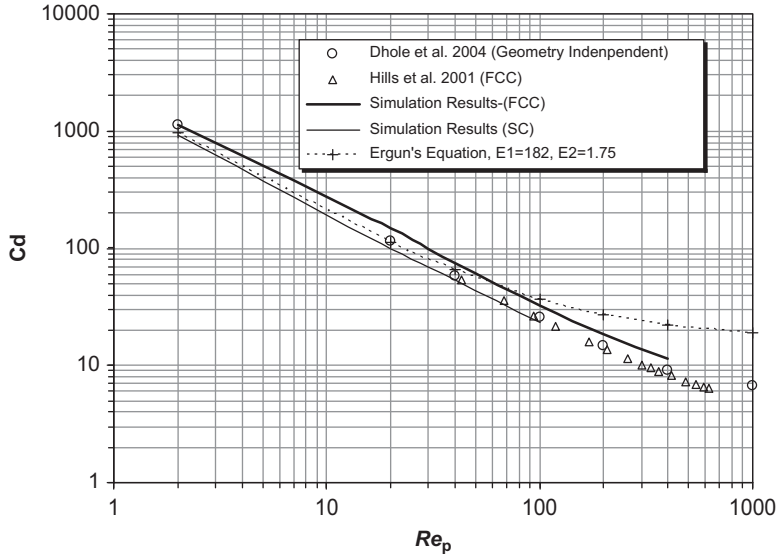

FIGURE 14 Comparison of simulated average drag coefficient with the literature data at various Reynolds numbers (Gunjal et al., 2005a).

geometrical orientation does not make a significant variation in overall drag force acting on the particle. However, the results of SC and one-dimensional rhombohedral geometry indicate that there is a significant difference in the predicted flow field distribution for these two cases. Figs. 9 and 13 also indicate that particle Reynolds number plays a significant role in the distribution of velocity inside the void space. Except the studies of Maier et al. (1998) and Magnico (2003) which report velocity distribution in void space at low Reynolds numbers, no other information is available in the literature on how particle arrangement and particle Reynolds number influence velocity distribution. The predicted distribution of z-velocity component is shown in Fig. 15 for one-dimensional rhombohedral geometry at different particle Reynolds numbers. At the lowest Reynolds number ($Re_p = 12.17$), z-velocity distribution exhibits a sharp peak and a shoulder. The predicted velocity distributions of rhombohedral arrangement are also similar to the results reported by Magnico (2003) and Maier et al. (1998). As the particle Reynolds number increases, the distribution broadens and becomes bi-modal. However, z-velocity distributions for three-dimensional rhombohedral geometry show different trends compared to the one-dimensional rhombohedral geometry (see Figs. 16 and 17). For three-dimensional rhombohedral geometry a flatter velocity distribution was observed at low as well as high Reynolds numbers.

Distributions of the axial component of velocity within the interstitial space for SC, rhombohedral (one-dimensional and three-dimensional), and FCC geometry were compared for Re_p 12.17 in Fig. 16. For SC and one-dimensional

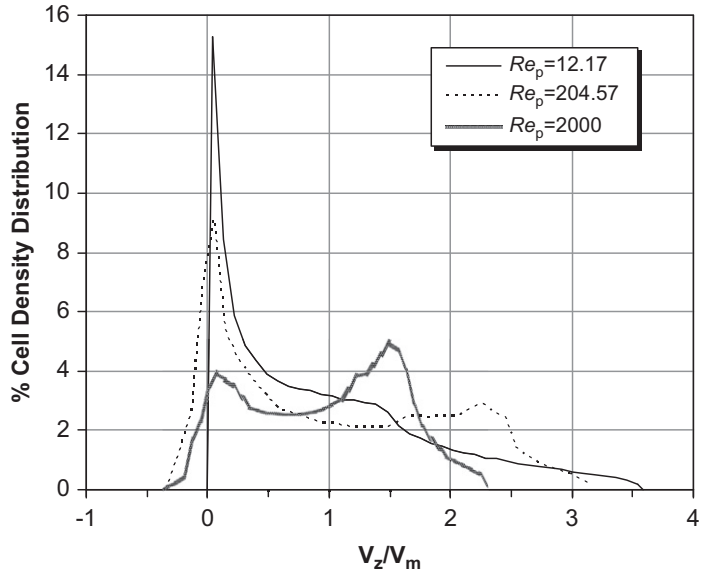

FIGURE 15 Histograms of z-velocity (axial velocity component) distribution obtained from simulations of liquid flow in one-dimensional rhombohedral cell at different Re_p (Gunjal et al., 2005a).

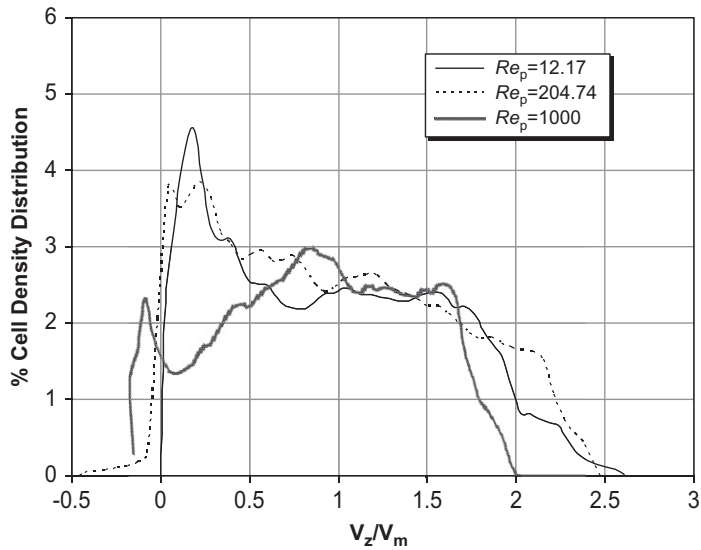

FIGURE 16 Histograms of z-velocity (axial velocity component) distribution obtained from simulations of liquid flow in three-dimensional rhombohedral cell at different Re_p (Gunjal et al., 2005a).

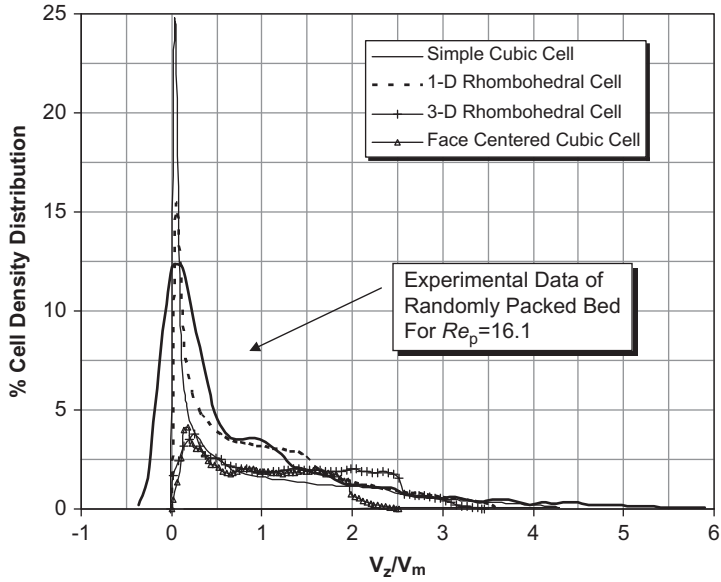

FIGURE 17 Histograms of z-velocity (axial velocity component) distribution obtained from simulations of liquid flow in different unit cells at $Re_p = 12.17$ and experimental data of Sederman et al. (1997) in randomly packed bed [$D = 4.7$ cm, $d_p = 5$ mm, normalized density distribution] (Gunjal et al., 2005a).

rhombohedral geometry, the predicted velocity distribution curves indicate that there are large numbers of cells containing low-magnitude axial velocities. However, for three-dimensional rhombohedral and FCC geometry a flatter velocity distribution was observed. Sederman et al. (1997) experimentally measured velocity distribution within the packed beds using MRI. Their data for the particle Reynolds number of 16.1 are also shown in Fig. 16. The velocity distribution obtained from experimental data of randomly packed bed lies between the trends observed in different arrangements considered here. Similar trends were observed in a predicted distribution of one of the transverse velocity components (x-velocity) in the interstitial space (see Fig. 18).

Total frictional resistance determined from the computational fluid dynamics (CFD) simulations showed good agreement with the values estimated using the Ergun equation (with $E_1 = 182$ and $E_2 = 1.75$) for all three packing arrangements. The Ergun equation was found to overpredict the drag coefficient for the turbulent flow regime. The ratio of surface drag to overall drag was almost independent of particle Reynolds number in the laminar flow regime. The values of this ratio obtained for the SC and FCC arrangements were almost the same (~0.21). For the rhombohedral arrangement (one-dimensional), the relative contribution of form drag was lower than that observed for the SC and FCC arrangements. The three-dimensional rhombohedral arrangement was

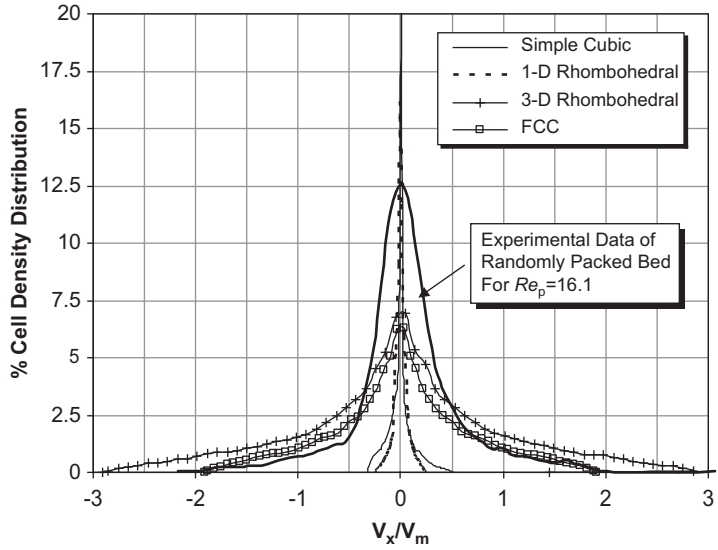

FIGURE 18 Histograms of x-velocity (transverse velocity component) distribution obtained from simulations of liquid flow in different unit cells at $Re_p = 12.17$ and experimental data of Sederman et al. (1997) in randomly packed bed ($D = 4.7$ cm, $d_p = 5$ mm, normalized density distribution) (Gunjal et al., 2005a).

found to offer maximum form drag. The predicted values of Nusselt numbers for the FCC arrangement showed reasonable agreement with the correlations of the particle to fluid heat transfer in packed beds. The predicted values of Nusselt number for the SC arrangement were much lower than those obtained for the FCC arrangement. Unlike the FCC, where flow impinges on the obstructing particle and changes directions several times within the "unit cell," no impingement and direction changes occur in the SC arrangement. This leads to significantly different path lines and velocity distribution and therefore the heat transfer. The unit cell approach can be used for quantitative understanding of influence of particle shapes and packing arrangement on flow and heat transfer.

Influence of Particle Shape on Flow Characteristics

Most of the results discussed so far were related to spherical particles. However, in practice several types of catalyst particles are used. For example, in cases where effectiveness factors are low, catalyst particles are "designed" to increase external surface area. Various types of catalysts have been designed with internal holes which increase surface area and bed porosity for improving performance (better catalyst activity and lower pressure drop). Some of these particle shapes are shown in Fig. 1 (of Chapter 1). Methodology of modeling of flow around an array of particles can be extended to particles of different shapes

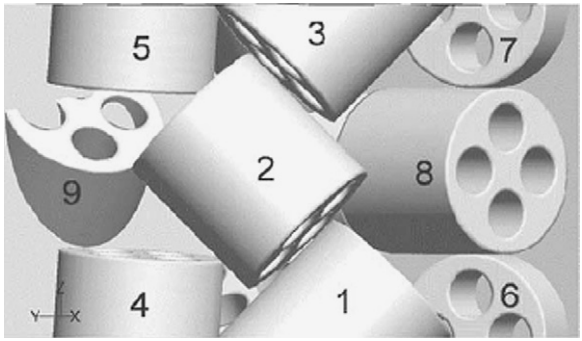

FIGURE 19 Assembly of cylindrical particles with holes considered by Nijemeisland, Dixon and Stitt (2004).

in a straightforward manner. As an example of this, a sample of results reported by Nijemeisland and Dixon (2004) is reproduced here. In their work, Nijemeisland and Dixon simulated flow and heat transfer over an assembly of particles of cylindrical shapes with internal holes (as shown in Fig. 19). Typical results are shown in Fig. 20. Path lines are colored by axial velocity in m/s. Dixon, Taskin, Nijemeisland, and Stit (2008) further extended this approach to quantify impact of particle shapes and packing on wall to particle heat transfer. It was observed that for comparable pressure drop costs, the multiholed particles lead to a lower tube wall temperature. The influence of changing diameter of holes for the four-small-holes and one-big-hole particles on flow and heat transfer was found to be rather small. The methodology and results discussed here can be used to guide design of catalyst particles for realizing better heat and mass transfer characteristics without incurring penalty of higher pressure drop. The approaches, models, and results discussed in this section are useful to gain better insight into flow within packed beds. The approaches and models used for simulating flow through larger packed beds are discussed in the following.

Flow Through a Packed Bed of Randomly Packed Particles

In the approach (A), as discussed earlier, instead of resolving individual particles in the packed bed, the entire packed bed region is treated as the porous media and flow through this media is simulated using averaged transport equations. This approach has been widely used to simulate flow through packed beds. For example, Ranade (1994) has used CFD model to optimize design of a deflector plate in an axial fixed-bed reactor. Foumeny and Benyahia (1993) also discussed application of CFD models for optimizing internals for axial flow fixed-bed reactors. Ranade (1997) has used this approach to improve the performance of radial flow packed bed reactor.

The key issue in modeling of fixed-bed reactor is the correct representation of a fixed bed (of solid particles) in a CFD model. In most of the cases, such

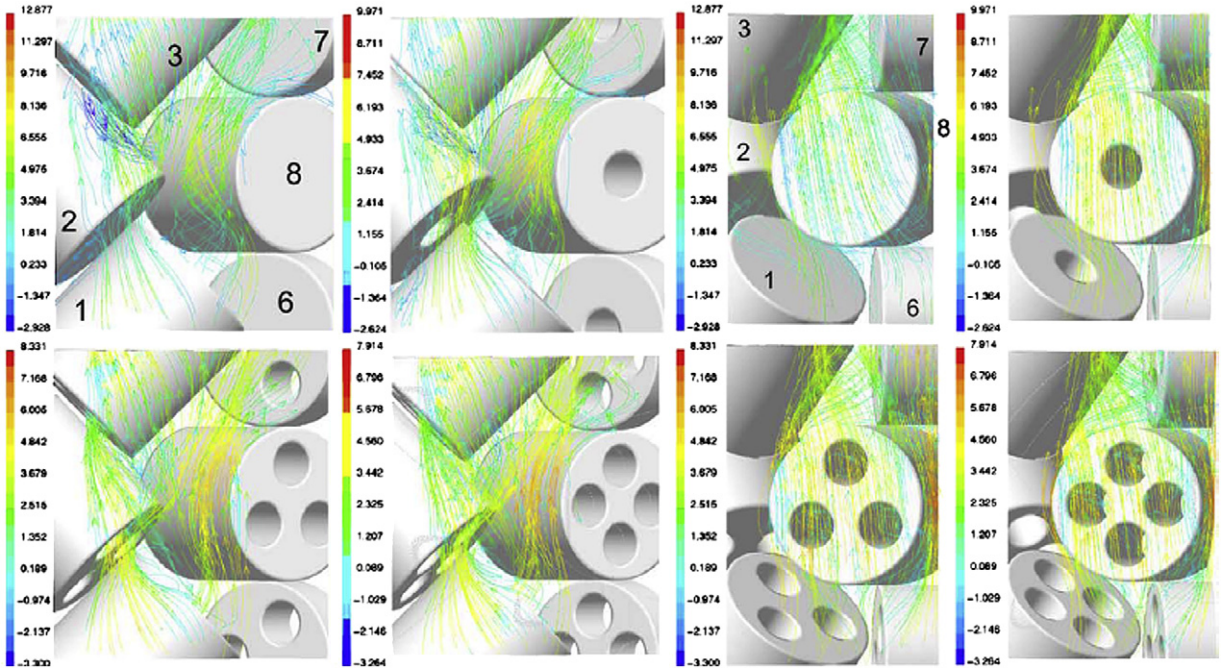

FIGURE 20 Comparison of flow situations related to particles with a different amount of holes; path lines are colored by axial velocity in m/s as per the scale shown on left side of the pictures (Nijemeisland, Dixon and Stitt, 2004).

a fixed bed of solid particles can be modeled as an isotropic or anisotropic porous media. Additional resistance offered by such porous media can then be modeled by introducing an additional momentum sink in the momentum transport equations. Usually additional resistance offered by porous media is represented in the flow model using two parameters, namely, permeability, α, and inertial coefficient, C_2. The additional momentum sink in terms of these two parameters is represented as:

$$\text{Momentum source} = -\left[\frac{\mu}{\alpha}V + C_2\left(\frac{1}{2}\rho V^2\right)\right] \tag{10}$$

Accuracy of such a representation obviously depends on the accuracy of the parameters used to represent the porous media. Best option to specify adequately accurate values of these parameters is, of course, experimental data. In the absence of such data, several correlations relating the pressure drop through porous beds and velocity and bed characteristics are available (see, for example, Carman, 1937; Ergun, 1952; Mehta & Hawley, 1969). The Ergun equation is one of the most widely used relations to represent the resistance of catalyst bed, which has the form:

$$\frac{\Delta P}{L} = \frac{E_1\mu}{d_p^2\phi_p^2}\frac{(1-\varepsilon)^2}{\varepsilon^3}V + \frac{E_2\rho}{d_p\phi_p}\frac{(1-\varepsilon)}{\varepsilon^3}V^2 \tag{11}$$

where $(\Delta P/L)$ is the pressure drop per unit length, μ is the viscosity, d_p is the equivalent pellet diameter, ϕ_p is the sphericity, ε is the porosity, and V is the superficial velocity. Where E_1 and E_2 are the Ergun's constants and are functions of bed characteristics. Ergun (1952) has recommended $E_1 = 150$ and $E_2 = 1.75$ for packed bed flow. Nemec and Levec (2005) have recently pointed out that these values of constants need to be modified to account for different particle shapes. The values of E_1 and E_2 increase with decrease in sphericity for cylindrical and polylobe particles. For estimating these constants as a function of sphericity for cylindrical, ring-shaped, and polylobe-shaped particles, correlations proposed by Nemec and Levec (2005) are recommended. The knowledge of pellet size, shape, and voidage of the bed are thus sufficient to characterize the resistance of the catalyst bed with the help of these correlations.

It must be noted that the porosity and its distribution in a packed bed are the key parameters in determining the flow distribution within the bed. Most of the correlations are usually obtained by considering parameters such as bed porosity averaged over the entire bed (ignoring spatial variation within the bed). Caution must be exercised in using such correlations for CFD simulations of flow through packed bed. In recent years, numerous attempts were made to provide quantitative information about the porosity distribution (see discussion in the section *Characterization of Packed Beds*). Mean porosity and its distribution are determined largely by particle size, shape,

surface properties, and method of packing. These experimental and computational studies have shown that the cross-sectional-averaged porosity along the height of the bed is distributed randomly and the longitudinally averaged radial porosity profile exhibits a maximum near the wall. Bed porosity was also found to fluctuate significantly in the near wall region (of width of about 4−5 particle diameters). The magnitude of fluctuations is a strong function of a ratio of column diameter to particle diameter (for $D/d_p > 15$, fluctuations are within 1% whereas for lower values of D/d_p, fluctuations may rise up to 30%). The correlation of Mueller (1991) discussed in the section *Characterization of Packed Beds* is fairly general and is recommended for using with the CFD models for flow through packed beds.

CFD simulations with such randomly distributed bed porosity can provide useful insights and help evolve guidelines for improving flow distribution in packed beds. This approach can also be used as a basis for simulating more complex gas−liquid flow through packed bed (discussed in the following section).

GAS−LIQUID FLOW THROUGH PACKED BEDS

The presence of liquid in addition to the gas phase flowing through the packed bed offers several additional challenges in the analysis of the flow behavior compared to those mentioned in the previous section. As discussed previously, porosity is not uniform in randomly packed beds. This implies that some flow channels, formed within a packed bed, offer less resistance to flow than other channels. Liquid will tend to move toward channels of lower resistance, leading to higher liquid holdup in such channels. Thus, even if the initial liquid distribution is uniform, inherent random spatial variation of the bed leads to non-uniform liquid flow. Wetting of solid particles of the bed by liquid is significantly influenced by surface characteristics, bed structure, contact angle, capillary forces, and flow rates of liquid and gas streams. It is important to capture these complex interactions among gas, liquid, and solid phases adequately while developing a model for gas−liquid flow through packed beds.

The modeling approaches discussed above are still applicable in general. The meso-scale approaches are useful for gaining better insight into interaction of gas and liquid phases with solid particles, especially wetting. The macroscopic models are useful to provide overall understanding and behavior of the entire bed. The meso-scale models are expected to provide a better understanding of the flow structure around particles and closure models which might be useful for macro-scale models. It will therefore be useful to discuss macroscopic approaches/models before discussing meso-scale models. The basic macro-scale and meso-scale modeling approaches and model equations are discussed in the following sections. Applications of these models are discussed in the subsequent section.

Modeling of Gas–Liquid Flow Through Packed Bed

Macro-scale Models

Several different approaches such as percolation theory approach (Crine, Marchot, & L'Homme, 1979), network model (Thompson & Fogler, 1997), the Eulerian–Eulerian approach with the multifluid models (Attou & Ferschneider, 1999; Grosser, Carbonell, & Sundaresan, 1988; Jiang, 2000; Yin, Sun, Afacan, Nandakumar, & Chung, 2000), and the lattice Boltzmann-type models (Mantle et al., 2001) have been applied to simulate gas–liquid flow in packed beds. Attou and Ferschneider (1999) and Grosser et al. (1988) have used one-dimensional flow model with uniform porosity distribution in the bed. The Eulerian–Eulerian approach with the two-dimensional multifluid models with spatial variation of the porosity appears to be most suitable for reactor engineering applications (Gunjal et al., 2005; Jiang, Khadilkar, Al-Dahhan, & Dudukovic, 2002; Kashiwa, Padial, Rauenzahn, & Vander-Heyden, 1994; Ranade, 2002). In this approach, continuum approximation is applied for all the phases. Volume-averaged mass and momentum balance equations for the k-th fluid can be written as:

Mass balance equation:

$$\frac{\partial \varepsilon_k \rho_K}{\partial t} + \nabla \cdot \varepsilon_k \rho_k U_k = 0 \tag{12}$$

Momentum balance equation:

$$\frac{\partial (\varepsilon_k \rho_k U_k)}{\partial t} + \nabla \cdot \left(\varepsilon_k \rho_k U_k U_k\right) = -\varepsilon_k \nabla P_k + \nabla \cdot (\varepsilon_k \mu \nabla U) + \varepsilon_k \rho_k g + F_{K,R}(U_k - U_r) \tag{13}$$

where, ε_k represents the volume fraction of each phase, ρ_k is the density of k-th phase, U_k is the cell velocity of k-th phase, and P is a mean pressure shared by all the phases present in the system. $F_{K,R}$ is an interphase (between k and r phases) momentum exchange term. Left-hand side of Eq. (13) represents the rate of change of momentum for the k-th phase. The right-hand side represents, pressure forces, gravitational acceleration, average shear stresses, and interphase momentum exchange. It is convenient to treat gas phase as a primary phase and liquid–solid phases as secondary phases. Solid phase should be considered as stationary and distribution of solid volume fraction can be assigned at the beginning of the simulation following the methods discussed in the previous section.

The pressure drop in the packed bed is usually correlated using the Ergun equation or its variants (Al-Dahhan & Dudukovic, 1994; Holub, Dudukovic,

& Ramachandran, 1992; Saez & Carbonell, 1985). Interphase coupling terms may therefore be formulated based on similar equations. The presence of liquid flow, however, leads to additional interphase exchanges, which need to be formulated correctly. Different approaches viz., relative permeability model (Grosser et al., 1988; Saez & Carbonell, 1985), slit model (Holub, Dudukovic, & Ramachandran, 1993), and two-fluid interaction model (Attou & Ferschneider, 1999, 2000) have been proposed to formulate interphase momentum exchange terms. The model of Attou and Ferschneider (1999), which includes gas–liquid interaction force, has a theoretically sound basis and is discussed here.

The model of Attou and Ferschneider (1999) was developed for the regime in which liquid flows in the form of a film. In this work, we have explored the possibility of using this model for simulating flow regimes in which part of the liquid may flow in the form of droplets. The interphase coupling terms $F_{K,R}$ (given here by Eqs. 14–16) proposed by Attou and Ferschneider (2000) are rewritten in terms of interstitial velocities and phase volume fractions as (instead of superficial velocities and saturation):

Gas–liquid momentum exchange term:

$$F_{\mathrm{GL}} = \varepsilon_{\mathrm{G}}\left(\frac{E_1\mu_{\mathrm{G}}(1-\varepsilon_{\mathrm{G}})^2}{\varepsilon_{\mathrm{G}}^2 d_{\mathrm{p}}^2}\left[\frac{\varepsilon_{\mathrm{S}}}{(1-\varepsilon_{\mathrm{G}})}\right]^{0.667} + \frac{E_2\rho_{\mathrm{G}}(U_{\mathrm{G}}-U_{\mathrm{L}})(1-\varepsilon_{\mathrm{G}})}{\varepsilon_{\mathrm{G}} d_{\mathrm{p}}}\left[\frac{\varepsilon_{\mathrm{S}}}{(1-\varepsilon_{\mathrm{G}})}\right]^{0.333}\right) \tag{14}$$

Gas–solid momentum exchange term:

$$F_{\mathrm{GS}} = \varepsilon_{\mathrm{G}}\left(\frac{E_1\mu_{\mathrm{G}}(1-\varepsilon_{\mathrm{G}})^2}{\varepsilon_{\mathrm{G}}^2 d_{\mathrm{p}}^2}\left[\frac{\varepsilon_{\mathrm{S}}}{(1-\varepsilon_{\mathrm{G}})}\right]^{0.667} + \frac{E_2\rho_{\mathrm{G}}U_{\mathrm{G}}(1-\varepsilon_{\mathrm{G}})}{\varepsilon_{\mathrm{G}} d_{\mathrm{p}}}\left[\frac{\varepsilon_{\mathrm{S}}}{(1-\varepsilon_{\mathrm{G}})}\right]^{0.333}\right) \tag{15}$$

Liquid–solid momentum exchange term:

$$F_{\mathrm{LS}} = \varepsilon_{\mathrm{L}}\left(\frac{E_1\mu_{\mathrm{L}}\varepsilon_{\mathrm{S}}^2}{\varepsilon_{\mathrm{L}}^2 d_{\mathrm{p}}^2} + \frac{E_2\rho_{\mathrm{L}}U_{\mathrm{G}}\varepsilon_{\mathrm{S}}}{\varepsilon_{\mathrm{L}} d_{\mathrm{p}}}\right) \tag{16}$$

It must be noted that a pressure shared by all the phases is used in momentum balance equation (Eq. 13). However, when two immiscible phases

are in contact with each other, interfacial tension causes the fluids to have different pressures. Such a pressure difference (capillary pressure) for gas and liquid phases may be written as:

$$P_G - P_L = 2\sigma\left(\frac{1}{d_1} - \frac{1}{d_2}\right) \tag{17}$$

where, d_1 and d_2 are the maximum and minimum diameters of the sphere with liquid film formed by the flowing liquid. More details of relating d_1 and d_2 to particle diameter, porosity, and the minimum equivalent diameter of the area between three particles in contact are given by Attou and Ferschneider (2000). Capillary pressure affects the liquid distribution and may set-up gradients of liquid holdup within the packed bed.

Several investigators have analyzed capillary forces (for example, Attou & Ferschneider, 2000; Grosser et al., 1988; Jiang et al., 2002; and references cited therein). Grosser et al. (1988) have studied onset of pulsing in trickle beds using linear stability analysis. Their analysis suggests that the competition between the inertial and capillary forces leads to a situation in which steady-state flow is not possible, implying the pulsing in trickle beds. Grosser et al. have proposed the capillary pressure as an empirical function of the liquid saturation:

$$P_L = P_G - \sigma\frac{\varepsilon_s E_1^{0.5}}{(1-\varepsilon_s)d_p}[0.48 + 0.036\ln(1-\beta_L)/\beta_L] \tag{18}$$

The order of magnitude analysis indicates that the magnitude of the capillary forces is rather small compared to the magnitudes of interphase drag forces. Attou and Ferschneider (2000) have obtained the following expression for the capillary pressure term based on geometric estimates of d_1 and d_2 and with empirical factor F to account for high pressure operations as:

$$P_G - P_L = 2\sigma\left(\frac{1-\varepsilon}{1-\varepsilon_G}\right)^{0.333}\left(\frac{5.416}{d_P}\right)F\left(\frac{\rho_G}{\rho_L}\right) \tag{19}$$

where,

$$F\left(\frac{\rho_G}{\rho_L}\right) = 1 + 88.1\frac{\rho_G}{\rho_L} \quad \text{for} \quad \frac{\rho_G}{\rho_L} < 0.025 \tag{20}$$

Under typical operating conditions of trickle beds, quantitative comparison of the capillary pressures estimated from Eqs. (18) and (19) is not very different (within 10%). Considering the geometric basis used by Attou and Ferschneider (1999), Eq. (19) is recommended for the macro-scale CFD model.

Pressure drop required to maintain specified gas and liquid throughputs is history dependent. Pressure drop at any specific liquid velocity measured with

increasing liquid velocity is more than that measured with decreasing liquid velocity (see, for example, Szady & Sundaresan, 1991). Capillary phenomenon is one of the contributing factors of this observation. Jiang et al., (2002) have attempted simulation of this phenomenon by introducing an empirical factor (f) related to the degree of wetting in their capillary pressure formulation as:

$$P_G - P_L = (1-f)P_c \tag{21}$$

For prewetted or fully wetted bed, f was set to one, implying zero capillary pressure. For non-wetted bed, f was set to zero (Jiang et al., 2002). For incorporating the capillary pressure in the CFD model, gradients of capillary pressure must be formulated as:

$$\frac{\partial P_G}{\partial z} - \frac{\partial P_L}{\partial z} = \frac{2}{3}\sigma \frac{5.416}{d_p}\left(\frac{\varepsilon_s}{1-\varepsilon_G}\right)^{-2/3}\left(\left(\frac{1}{1-\varepsilon_G}\right)\frac{\partial \varepsilon_s}{\partial z} + \left(\frac{\varepsilon_s}{(1-\varepsilon_G)^2}\right)\frac{\partial \varepsilon_G}{\partial z}\right)F\left(\frac{\rho_G}{\rho_L}\right) \tag{22}$$

Equation (22) can be used to express the gradients of liquid pressure (P_L) in the liquid phase momentum equations in terms of gradients of gas pressure (P_G) to incorporate the capillary pressure terms.

The model equations described above can be solved numerically with appropriate boundary conditions. Porosity distribution within the bed can be specified using the methods described while discussing single-phase flow through packed beds. At the inlet, velocity boundary conditions may be used. It is generally useful to minimize the discontinuity at the inlet. This can be accomplished by specifying the inlet boundary conditions based on estimated value of the overall liquid volume fraction, $\langle \varepsilon_L \rangle$ as:

$$U_{Lin} = \frac{(V_L/\rho_L)}{\langle \varepsilon_L \rangle} \quad U_{Gin} = \frac{(V_G/\rho_G)}{1-\langle \varepsilon_L \rangle} \tag{23}$$

where V_L and V_G are mass fluxes of liquid and gas phases (kg/m^{2}s), respectively, and ρ_L and ρ_G are densities of liquid and gas, respectively. No slip boundary condition can be used for all the impermeable walls.

Application of such macro-scale models for simulating trickle bed reactors involves extending these equations for considering species transport and chemical reactions. These extensions are discussed in a separate sub-section on *Simulation of Reactions in Trickle Bed Reactors*.

Meso-scale Models

Some of the important issues in macroscopic modeling of gas–liquid flow through packed beds are closure models for interphase drag, wetting, and capillary forces. It is essential to understand how liquid interacts with solid

surfaces (either flat or curved) to make progress. One of the simplest "model" problem to understand such interactions is the interaction of liquid drops with flat and curved surfaces. The phenomenon of spreading of liquid drop on flat solid surface has been studied extensively (Gunjal, Chaudhari, & Ranade, 2005b and references cited therein).

Several methods are available to simulate free-surface flows (Fukai et al., 1995; Fukai, Zhao, Poulikakos, Megaridis, & Miyatake, 1993; McHyman, 1984; Monaghan, 1994; Ranade, 2002; Unverdi & Tryggvason, 1992) and motion of gas−liquid−solid contact line on solid surfaces. Free-surface methodologies can be classified into surface tracking, moving mesh, and fixed mesh (volume tracking) methods. Surface tracking methods define a sharp interface whose motion is followed using either a height function or marker particles. In moving mesh methods, a set of nodal points of the computational mesh is associated with the interface. The computational grid nodes are moved by interface fitted mesh method or by following the fluid. Both of these methods retain the sharper interface. However, mesh or marker particles have to be relocated and re-meshed when interface undergoes large deformations. As the free-surface deformation becomes complex, the application of these methods becomes computationally very intensive. Another method, which can retain a sharp interface, is the boundary integral method (Davidson, 2000, 2002). However, use of this method is still mainly restricted to two-dimensional simulations.

Volume of the fluid (VOF) method developed by Hirt and Nichols (1981) is one of the most widely used methods in modeling of free surfaces. This is a fixed mesh method, in which, the interface between immiscible fluids is modeled as the discontinuity in characteristic function (such as volume fraction). Several methods are available for interface reconstruction such as SLIC (simple line interface calculation), PLIC (piece-wise linear interface calculations), and Young's PLIC method with varying degree of interface smearing (Ranade, 2002; Rider & Kothe, 1995; Rudman, 1997; for more details). The governing equations and other associated closure models may be found elsewhere (for example, Gunjal et al., 2005b; Lopes & Quinta-Ferreira, 2009; Ranade, 2002; and references cited therein). This approach has been used for quantitative understanding of spreading of liquid film and interaction of droplets with flat and curved surfaces (see, for example, Gunjal et al., 2005b).

The flow field predicted by the VOF models can be used to examine various intricate details of interaction of a liquid drop and flat surface. Gunjal et al. (2005b) have demonstrated this by critically analyzing variation of kinetic, potential, and surface energies during drop impact, spreading, and oscillation processes. When a drop spreads to its maximum extent and is about to recoil, its potential energy exhibits minimum. For every cycle of potential energy, there are two cycles of kinetic energy because it passes through maximum during spreading as well as recoiling. Scales of variation

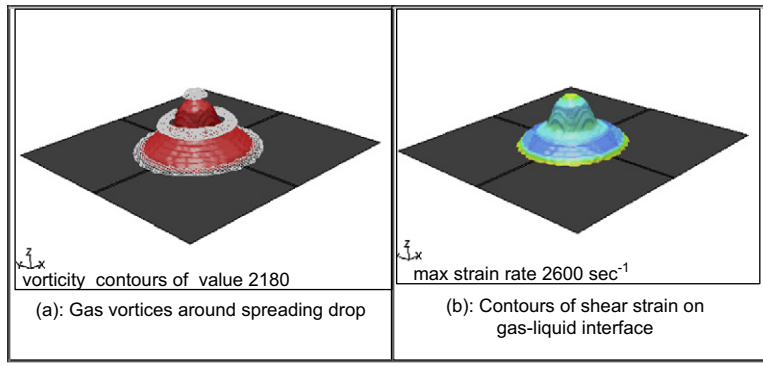

FIGURE 21 Illustration of gas–liquid and liquid–solid interactions during drop spreading on glass surface at time = 7.5 ms (Gunjal, Chaudhari, & Ranade, 2005b). System: 3 mm water drop with impact velocity 0.3 m/s on glass surface of static contact angle 64°. (a) Gas vortices around spreading drop; (b) contours of shear strain on gas–liquid interface.

of surface energy are higher than the potential and kinetic energy and its variation is very sensitive to the variation in a contact angle. Therefore, small errors in the values of contact angle or surface area may corrupt the calculation of total energy. The detailed flow field predicted by such VOF simulations can be used to compute other quantities of interest such as gas–liquid and liquid–solid interactions (as shown in Fig. 21). Liquid–solid interaction can be determined by calculating the average shear stress exerted by the fluid on the solid surface (see Fig. 21). Gas–liquid interaction can be studied by calculating the strain rate on gas–liquid interface. Detailed study of gas–liquid interaction (in terms of strain rate), gas recirculation (in terms of vorticity) as illustrated in Fig. 21 will be useful for understanding interphase heat, mass, and momentum transfer in such flows. Maximum drop interfacial area was observed when the drop spreads completely; strain rate is smallest at this point. Microscopic evaluation of these parameters would be eventually useful for developing better closure terms for macro-scale flow models.

Recently Lopes and Quinta-Ferreira (2009) have used VOF approach to simulate gas–liquid flow through an array of solid particles. The computational model was used to quantify effect of gas and liquid flow rates on frictional pressure drop and liquid holdup. Some of the results obtained by them are reproduced in Figs. 22–26. The meso-scale models with VOF approach capture complex interactions of gas–liquid–solid phases reasonably well (at least for low gas velocities).

These meso-scale models can in principle provide useful quantitative information for developing closure models for the macro-scale simulations. These models can also help extrapolating our understanding and data for higher temperatures and pressures relevant to industrial trickle bed reactors.

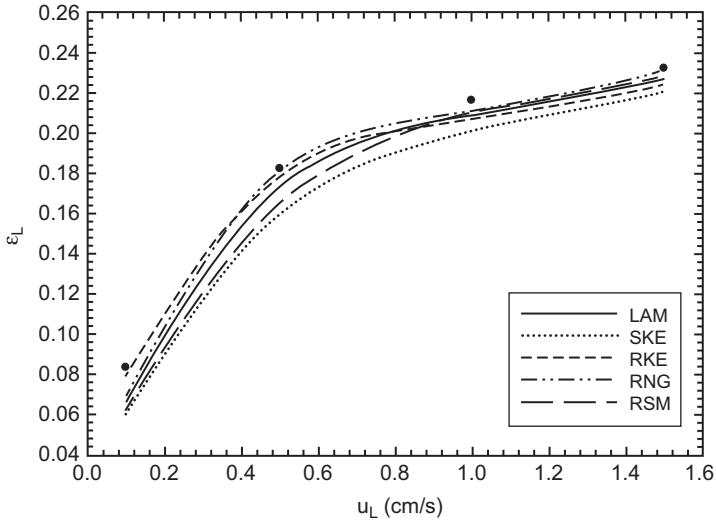

FIGURE 22 Influence of turbulence model on liquid holdup predictions at $G = 0.1$ kg/m^{2}s (Lopes & Quinta-Ferreira, 2009).

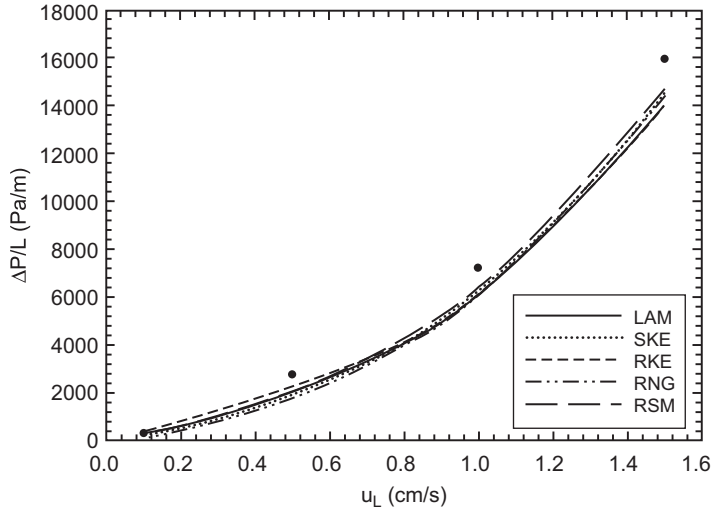

FIGURE 23 Influence of turbulence model on pressure drop predictions at $G = 0.1$ kg/m^{2}s (Lopes & Quinta-Ferreira, 2009).

Further work using this approach is needed for creating a comprehensive basis for selecting appropriate closure models for the macro-scale simulations. A sample of results obtained with the macro-scale models is discussed in the following.

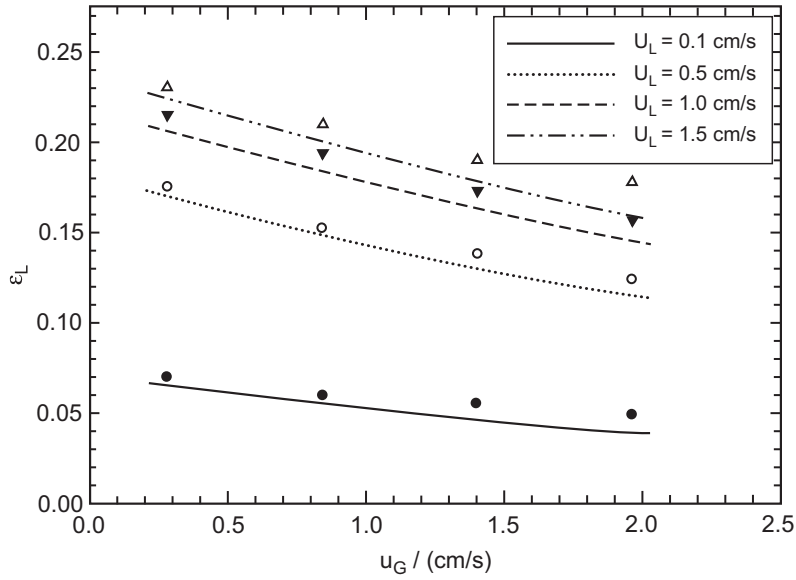

FIGURE 24 Influence of gas and liquid velocities on liquid holdup predictions (Lopes & Quinta-Ferreira, 2009).

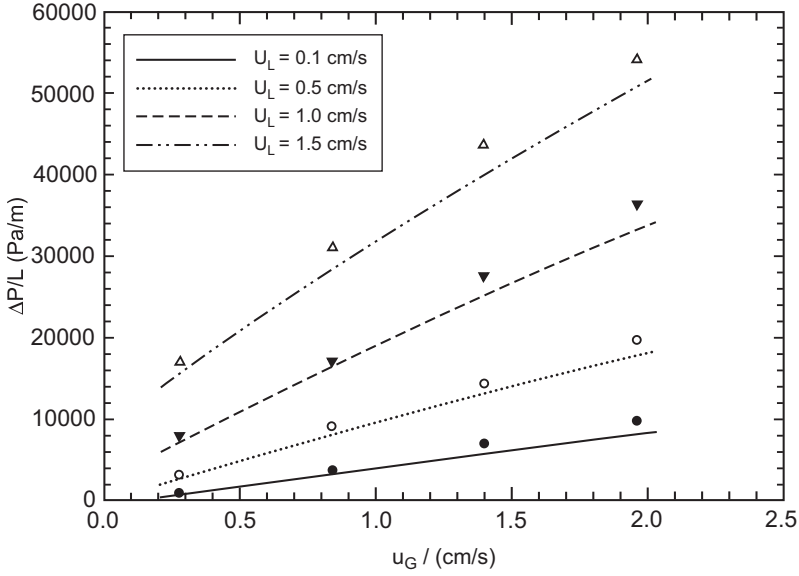

FIGURE 25 Influence of gas and liquid velocities on pressure drop predictions (Lopes & Quinta-Ferreira, 2009).

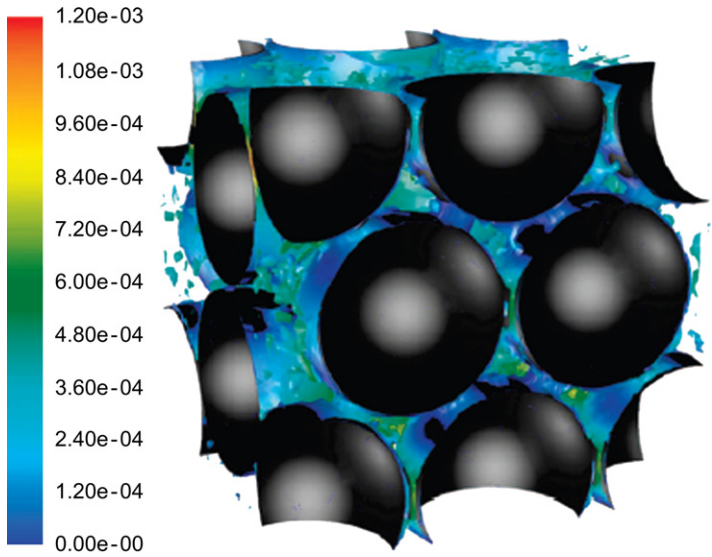

FIGURE 26 Instantaneous snapshot of liquid holdup isosurface (el = 0.15) colored by liquid velocity magnitude [$L = 5$ kg/m^{2}s, $G = 0.7$ kg/m^{2}s, $P = 30$ bar, $d_p = 2$ mm] (Lopes & Quinta-Ferreira, 2009).

Simulation of Gas–Liquid Flow in Trickle Beds

Recently, Gunjal et al. (2005) reported experimental data and CFD results on trickle beds of two different diameters with two particle sizes. Some of their results are reproduced here to illustrate the application of CFD model for simulating macro-scale flow characteristics in a trickle bed. The CFD model was then used to estimate the extent of suspended liquid in trickle flow regime and to simulate periodic operation of trickle beds to seek an insight into the pulse flow regime.

As discussed earlier, measurements of pressure drop and liquid holdup for trickle bed reactor showed hysteresis with liquid velocity. The observed hysteresis is associated with the capillary pressure acting on three-phase contact line. Accurate representation of capillary term in CFD model is difficult. The simulations were carried out by setting value of "f" from Eq. (21) to one for prewetted beds and to zero for a dry bed. The simulated results are compared with the experimental data in Figs. 27 and 28. As observed in the experiments, simulated results showed lower pressure drop for the dry bed compared to the prewetted bed. The predicted magnitude of the hysteresis is, however, lower than that observed in the experiments. For the dry bed (lower branch as well as the initial part of the upper branch), experimental data showed non-linear variation of pressure drop with liquid velocity. However, simulated results showed almost a linear variation. The inadequate representation of

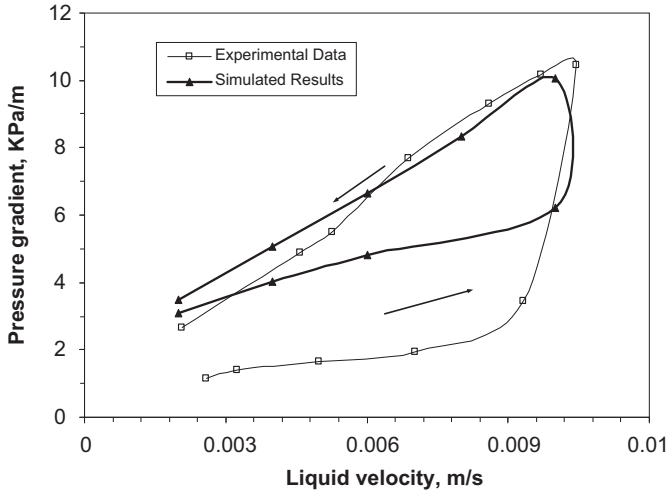

FIGURE 27 Comparison of simulated results of pressure drop for prewetted and non-prewetted beds [$V_G = 0.22$ m/s, std dev = 5%, $D = 0.114$ m, $d_p = 3$ mm] (Gunjal et al., 2005).

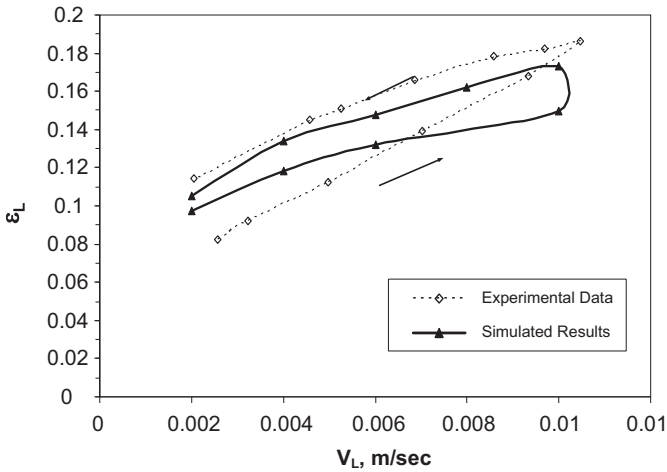

FIGURE 28 Comparison of simulated results of liquid holdup for prewetted and non-prewetted beds [$V_G = 0.22$ m/s, std dev = 5%, $D = 0.114$ m, $d_p = 3$ mm] (Gunjal et al., 2005).

capillary forces is the most likely cause of this discrepancy. Non-linearity appears even in upper branch mainly because, when liquid velocity is reduced, partial dryout may occur in the bed making it similar to the non-prewetted bed. Simulated contours of liquid holdup for prewetted bed and non-prewetted bed are shown in Fig. 29. Liquid distribution in prewetted bed is relatively uniform as compared to the non-prewetted bed conditions (Fig. 29). It can be seen from

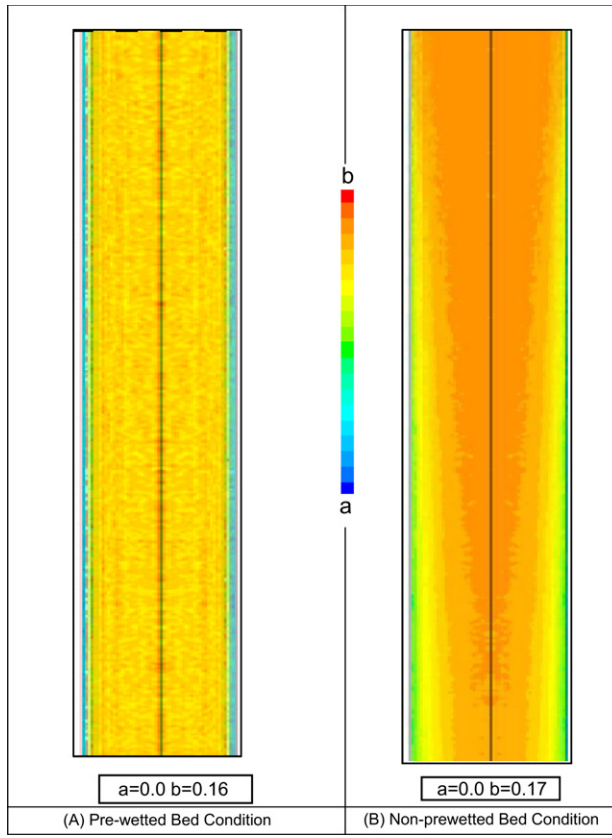

FIGURE 29 Simulated contours of liquid holdup for prewetted and non-prewetted bed [$V_L = 6$ kg/m^{2}s, $V_G = 0.22$ m/s, std dev = 5%, $D = 0.114$ m, $d_p = 3$ mm] (Gunjal et al., 2005). (A) Prewetted bed condition; (B) non-prewetted bed condition.

Fig. 30 that velocity and holdup distributions within the bed for liquid phase for prewetted and non-prewetted beds are substantially different. Distributions for the prewetted bed are wider than non-prewetted bed.

For prewetted bed, simulated results of pressure drop for the 0.114 m diameter of column are compared with the experimental data (Fig. 31) for gas velocities 0.22 m/s and 0.44 m/s. Simulated results overpredict pressure drop for 3 mm particle at low gas velocity (0.22 m/s) and underpredict for high gas velocity ($V_G = 0.44$ m/s). However, for 6 mm particles, simulated results show reasonable agreement with the experimental data. The disagreement at low liquid velocity for $V_G = 0.44$ m/s may be due to dryout phenomenon at high gas flow rate. Influence of column diameter on the agreement between simulated and experimental data is shown in Fig. 32. It can be seen that the agreement is better for 6 mm particles than for 3 mm particles. One of the possible reasons

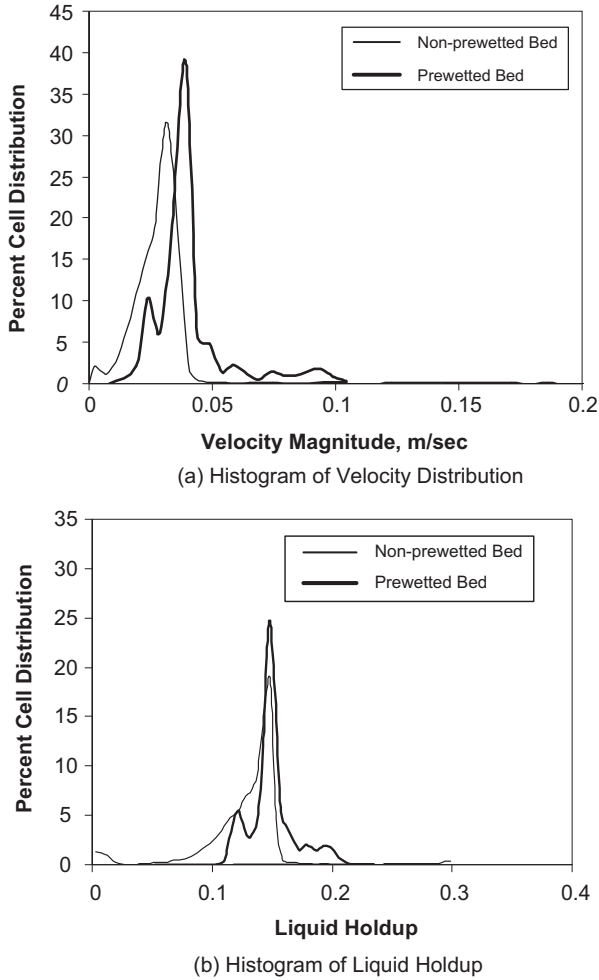

FIGURE 30 Simulated results of liquid velocity and holdup (Gunjal et al., 2005). (a) Histogram of velocity distribution; (b) histogram of liquid holdup.

for this could be inadequacies in representation of appropriate porosity distribution for 3 mm particle. Simulated values of the total liquid holdup in column of 0.114 m diameter are compared with the experimental data in Fig. 33. Simulated results show good qualitative as well as quantitative agreement with the experimental data. Similar agreement was also found for liquid holdup in 0.194 m diameter column (see Fig. 34). The simulated results can also be used to gain an insight in to hydrodynamics of gas−liquid flow through trickle beds.

In order to illustrate the application over a wider range of operating conditions, the simulations of three independent experimental data sets carried

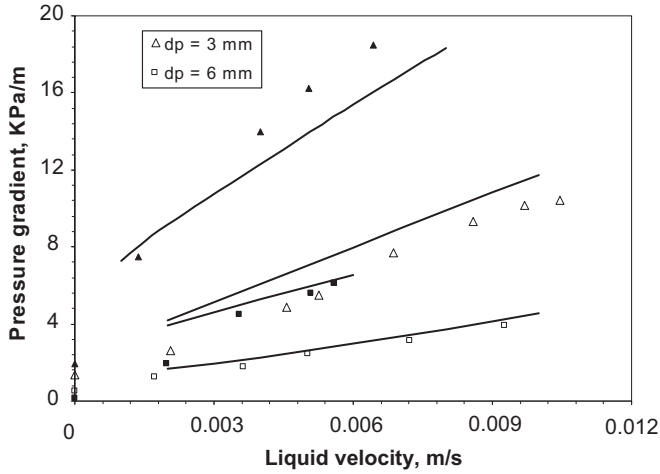

FIGURE 31 Comparison of CFD results with experimental data (Gunjal et al., 2005). Filled symbols: $V_G = 0.44$ m/s. Unfilled symbols: $V_G = 0.22$ m/s, $D = 0.114$ m.

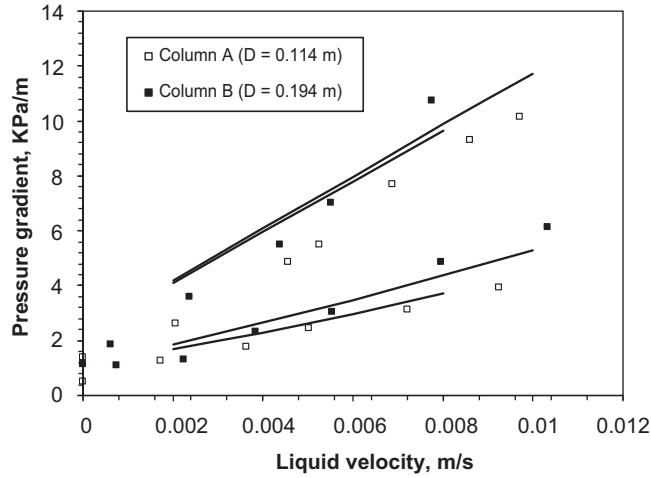

FIGURE 32 Comparison of CFD results with experimental data with $d_p = 3$ mm (Gunjal et al., 2005). Filled symbols: $V_G = 0.44$ m/s. Unfilled symbols: $V_G = 0.22$ m/s.

out by Gunjal et al. (2005) are briefly discussed here. Details of bed characteristics and operating conditions used in these three cases are summarized in Table 1. In Case 1, column to particle diameter (D/d_p) ratio was much higher compared to the other two cases. In Case 1 variation of pressure drop and liquid saturation was studied with change in liquid mass flow rate, while effect of change in gas mass flow rate on hydrodynamic parameters was studied in the other two cases. Gas mass flow rate in Case 3 was much higher than the other

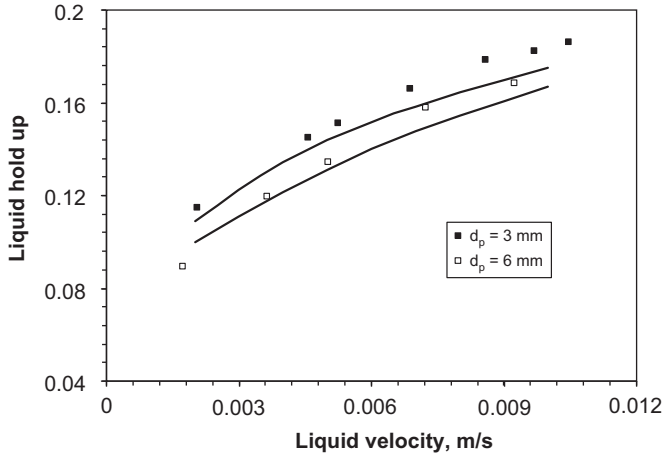

FIGURE 33 Comparison of CFD results with experimental data (Gunjal et al., 2005) [$D = 0.114$ m, $V_G = 0.22$ m/s].

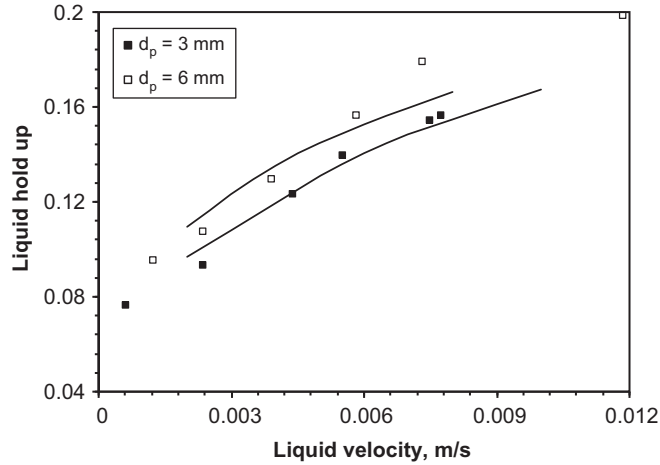

FIGURE 34 Comparison of CFD results with experimental data (Gunjal et al., 2005) [$D = 0.194$ m, $V_G = 0.22$ m/s].

two cases. Comparison of the experimental data with the simulated results is discussed in the following section.

Comparison of simulated results with the experimental data of Szady and Sundaresan (1991) for pressure drop and total liquid saturation is shown in Fig. 35a (only upper branch of pressure drop curve is shown here). The predicted results showed the correct trends of variation of the pressure drop and liquid saturation with liquid mass flow rate. The values of Ergun's (E_1 and E_2)

TABLE 1 Details of Bed Characteristics and Operating Conditions Used in Simulations

Case	Data Source	D/d_p	Bed Characteristics	V_G (m/s)	$V_L \times 10^3$ (m/s)	Ergun's Constants (E_1 and E_2)
1	Szady and Sundaresan (1991)	55	3 mm spherical; $\varepsilon_B = 0.37$	0.22	0.2−0.8	215 and 1.75
2	Specchia and Baldi (1977)	29.6	2.7 mm spherical; $\varepsilon_B = 0.38$	0.2−0.8	2.8	500 and 3
3	Rao et al. (1983)	15.4	3 mm spherical; $\varepsilon_B = 0.37$	1.5−5.5	1.0	215 and 3.4

constants used in the closure models represent the bed packing characteristics. In this case, $E_1 = 215$ and $E_2 = 1.75$ were used for carrying out the simulations. At low liquid velocities, the model showed good agreement with the experimental data. At higher liquid velocities (~8 kg/m^{2}s), model underpredicted the pressure drop values. This may be because of the possible transition from trickle flow regime to pulse flow regime. Model predictions for pressure drop and liquid saturation for experimental data of Specchia and Baldi (1977) is shown in Fig. 35b. In this case, higher values of Ergun's constants ($E_1 = 500$ and $E_2 = 3$) were used in the model. These values are close to the values suggested by Holub et al. (1992). In this case, model predictions showed good agreement with the experimental data of pressure drop and liquid saturation. A third set of data from Rao, Ananth, and Varma (1983), which was obtained for very high gas velocities compared to earlier data sets (1−8 kg/m^{2}s), was also used for evaluating the model predictions. As velocity of the gas phase increases (>1.5 kg/m^{2}s), trickle flow regime may change to spray flow regime. It can be seen from Fig. 35c that the model predictions showed good agreement with the experimental data for the high gas velocity cases as well (with $E_1 = 215$ and $E_2 = 3.4$). Though, the value of E_2 looks rather high, it is well within the range of values used by previous investigators (see a review given by Holub et al., 1992).

The simulated results show reasonable agreement with the experimental data of various studies. The basic CFD model developed in this work uses two parameters (E_1 and E_2) to match the predicted pressure drop with the reported experimental data. Reported results indicate that with appropriate values of these parameters, CFD model is able to predict the overall liquid saturation

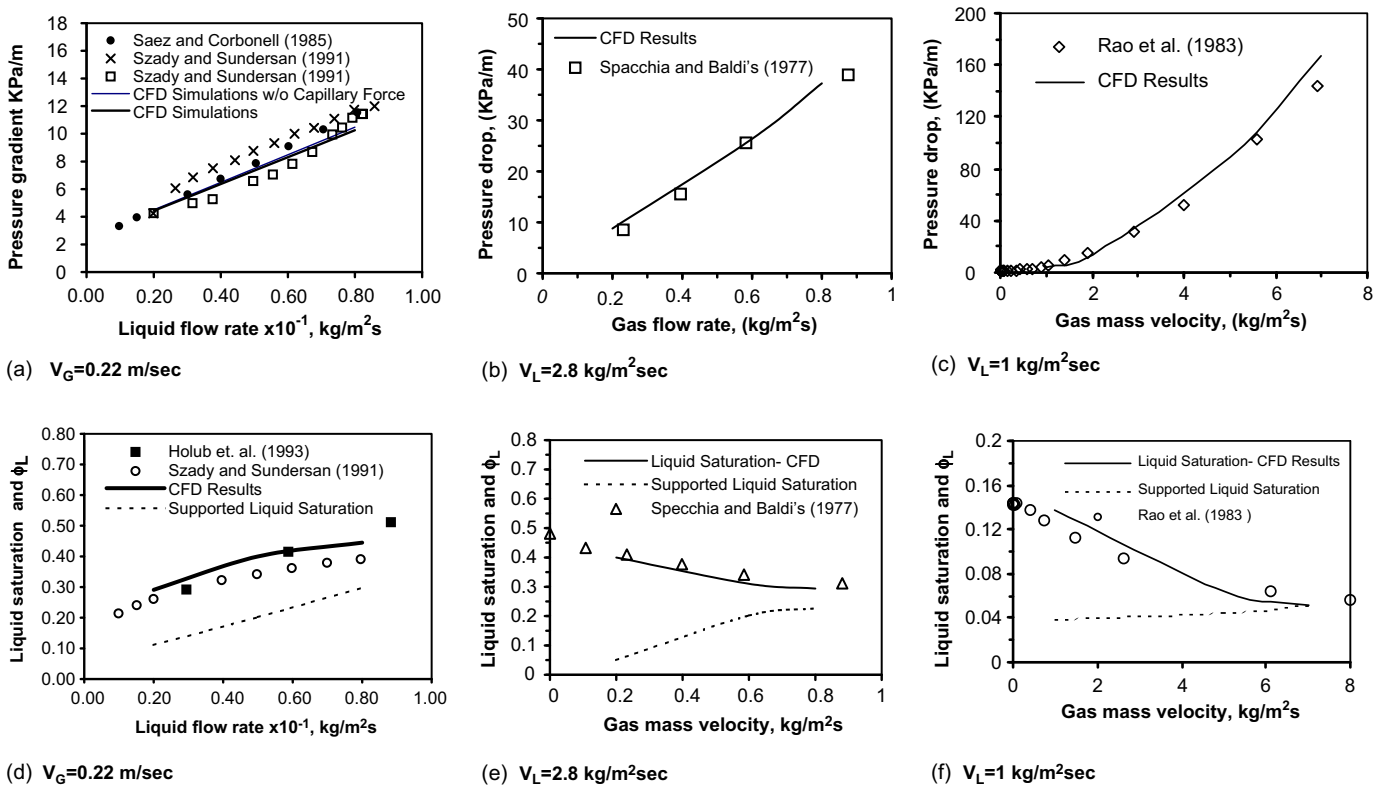

FIGURE 35 Comparison of simulated pressure drop and liquid saturation with the literature data (Gunjal et al., 2005). (a) $V_G = 0.22$ m/s; (b) $V_L = 2.8$ kg/m^{2}s; (c) $V_L = 1$ kg/m^{2}s; (d) $V_G = 0.22$ m/s; (e) $V_L = 2.8$ kg/m^{2}s; (f) $V_L = 1$ kg/m^{2}s. Other details of three experimental sets are listed in Table 1.

correctly for the range of gas and liquid velocities. Encouraged by such an agreement, the CFD model developed here was used to estimate frictional pressure drop and supported liquid saturation. For this purpose, simulations were carried out for two values of gravitational acceleration. For the detailed procedure to calculate the frictional pressure drop and supported liquid holdup, the reader is referred to the paper by Gunjal et al. (2005).

Following their procedure, frictional pressure drop and liquid saturation supported by gas phase were calculated. The predicted values of supported liquid saturation are shown by a dotted line in Fig. 35d–f. Figure 35d shows that fraction of liquid supported by gas phase increases with liquid velocity. The results shown in Fig. 35e and f indicate that the fraction of supported liquid saturation increases with gas velocity though increase in gas velocity decreases total liquid holdup or saturation. At very high gas velocity (see Fig. 35f) almost all the liquid holdup is supported by gas phase, indicating a spray flow regime. Thus, the procedure of Gunjal et al. (2005) can be used to estimate fraction of liquid supported by the gas phase and to identify possible transition to a spray flow regime.

In many industrial practices, liquid-induced periodic operations are preferable because reactor operation with natural pulsing is difficult for large reactors. It is worthwhile to apply present CFD model to simulate periodic operation of a trickle bed. This will also help to gain an insight into the features of the pulse flow regime. In natural pulse flow regime, liquid-enriched pulses form after some distance from the inlet and they accelerate while moving downward. Formation of pulses is associated with complex interactions among capillary forces, wall adhesion, and the convective forces. If the model equations adequately represent this underlying physics and numerical solution does not add any artificial diffusivity, the simulated results should be able to capture transition from trickle flow regime to pulse flow regime. However, the current understanding of physics of pulse formation and its implementation in CFD model is not adequate for this purpose. Alternative way to gain some insight into pulse-like flow in trickle beds is to simulate periodic operation of trickle beds with induced pulses by manipulating inlet liquid velocity. Boelhouwer, Piepers, and Drinkenburg (2002) have compared the key features of natural pulsing and induced pulsing trickle beds. Their results showed that the variation between natural pulsing and induced pulsing is within 25%. Following this, Gunjal et al. (2005) had simulated flow in trickle beds operated with liquid-induced pulsing maintaining the same average flow rates. The frequency of liquid-induced pulsing was set from the experimental measurements of natural pulsing. They carried out simulations of liquid-induced periodic operation for different liquid flow rates ($V_L = 11-24\ \mathrm{kg/m^2s}$) at a gas flow rate of $V_G = 0.22$ m/s. The predicted pressure drop was not found to be sensitive to the pulsing frequency within the range studied. The models discussed in this section can, however, be used to simulate periodic operation of trickle bed reactor as well.

Simulation of Reactions in Trickle Bed Reactors

CFD models can be used to simulate liquid phase mixing and reactions in trickle bed reactors. Ability to represent porosity variation within the bed and to consider detailed three-dimensional configurations of real-life reactors offers new possibilities of gaining insight and of improving performance of such industrial reactors. For extending the CFD models described earlier to simulate liquid phase mixing and reactions, species mass balance equations need to be solved in addition to the overall mass, momentum, and energy conservation equations. These additional species conservation equations are of the form:

$$\frac{\partial \varepsilon_k \rho_k C_{k,i}}{\partial t} + \nabla \cdot \left(\varepsilon_k \rho_k U_k C_{k,i}\right) = \nabla \left(\varepsilon_k \rho_k D_{i,m} \nabla C_{k,i}\right) + \varepsilon_k \rho_k S_{k,i} \tag{24}$$

where, $C_{k,i}$ is the concentration of species i in k-th phase (gas or liquid) and ρ_k and ε_k are the density and volume fraction of the k-th phase, respectively. $S_{k,i}$ is the source for species i in phase k.

The formulation of source terms depends on gas–liquid, gas–solid, and liquid–solid mass transfer, extent of wetting of particles, extent of intraparticle concentration profiles, and reaction kinetics. The source term for species i in gas phase can be written as:

$$S_i = -k_{\mathrm{GL}i} a_{\mathrm{GL}} \left[\frac{C_{\mathrm{G}i}}{H_i} - C_{\mathrm{L}i}\right] - k_{\mathrm{GS}i} a_{\mathrm{GS}} [C_{\mathrm{G}i} - C_{\mathrm{S}i}] \tag{25}$$

where "k" denotes mass transfer coefficient and "a" denotes interfacial area per unit volume of the reactor. The subscripts GL and GS denote gas to liquid and gas to solid, respectively. It should be noted that a_{GS} will be zero if particles are completely wetted (that is, when gas phase is not directly in contact with the solid particles). The corresponding source term for species i in liquid phase may be written as,

$$S_i = k_{\mathrm{GL}i} a_{\mathrm{GL}} \left[\frac{C_{G\mathrm{i}}}{H_i} - C_{\mathrm{L}i}\right] - k_{\mathrm{LS}i} a_{\mathrm{LS}} [C_{\mathrm{L}i} - C_{\mathrm{S}i}] \tag{26}$$

where subscript LS denotes liquid to solid. The unknown solid concentrations are calculated by assuming no accumulation on solid as:

$$k_{\mathrm{GS}i} a_{\mathrm{GS}} [C_{\mathrm{G}i} - C_{\mathrm{S}i}] + k_{\mathrm{LS}i} a_{\mathrm{LS}} [C_{\mathrm{L}i} - C_{\mathrm{S}i}] = \rho_{\mathrm{B}} \sum_{j=1}^{j=\mathrm{nr}} \eta_{oj} r_{ij} \tag{27}$$

where, r is the rate of reaction in consistent units (kg/kg of catalysts), nr is the number of reactions, and ρ_{B} is the catalyst bulk density of the bed, kg of catalyst/m^3 of bed. η_{oj} is the overall catalyst particle effectiveness factor (weighted average of wetted and unwetted portion) for reaction j.

Physico-chemical properties of the systems (like density, viscosity, heat capacity, etc.) will in general be functions of species concentration and temperature. Appropriate correlations to estimate these properties can be incorporated in the CFD framework following standard practices (see Ranade, 2002 for more details). For interphase mass and heat transfer, appropriate correlations need to be selected (see Chapter 2 for discussion on various correlations which may be used for this purpose). With some of these empirical correlations, CFD models allow simulation of various key parameters like liquid holdup and its distribution within the bed and RTD without any further empiricism. This avoids the need of approximating liquid phase mixing (use of correlations to estimate dispersion coefficient) and liquid holdup/distribution. These types of CFD models have been shown to capture liquid phase mixing and reactions in trickle bed reactor reasonably well. For example, Gunjal, Ranade, and Chaudhari (2003) simulated liquid phase RTD using a similar model. Comparison of predicted RTD with the experimental data is shown in Fig. 36. Predicted RTD response is reasonably close to the experimental values. The CFD models can capture influence of porosity variation within the bed as well as key design issues and hardware details like location and sizing of inlet nozzles, supports, and distributors on hydrodynamics and therefore on reactor performance. Application of the models discussed here for simulating laboratory-scale and commercial-scale hydroprocessing reactors is discussed in Chapter 6. Application of Chapters 2–4 for reactor performance evaluation and scale-up is discussed in Chapter 5.

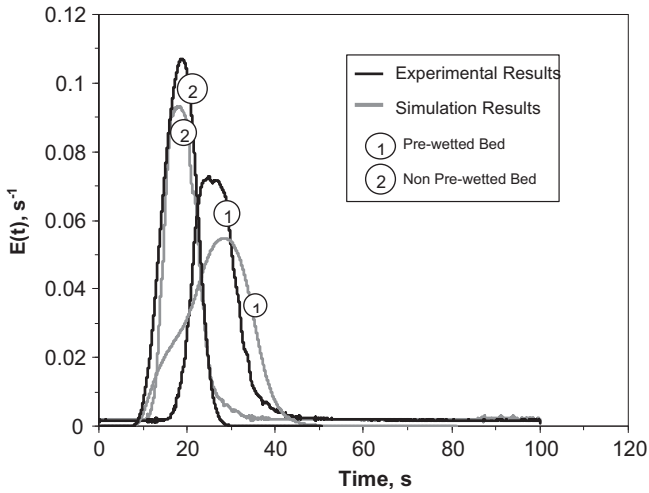

FIGURE 36 Comparison of the predicted residence time distribution with the experimental data (Gunjal et al., 2003). System: $D = 0.114$ m, $d_p = 6$ mm, $V_L = 1.72$ kg/m^{2}s, $V_G = 0.22$ m/s, std. dev. $= 5\%$, $d_p = 6$ mm, $E_1 = 500$, and $E_2 = 3.4$.

SUMMARY

Ability to predict and control the underlying fluid dynamics is essential to gain an insight for developing innovative engineering solutions. With the current level of understanding, it is more advantageous to use hierarchy of models coupled with key experimental findings to achieve practical benefits. In this chapter, therefore, different modeling approaches which allow better quantitative understanding of the processes occurring in trickle bed reactors are discussed. Different approaches for simulating single-phase flow through packed bed were first discussed. A "unit cell" approach or considering an assembly of few particles is very useful for obtaining quantitative insights into flow structures and transport processes occurring in packed beds. This approach can also be extended to gas–liquid flow through packed beds using VOF (volume of fluid) models. Information obtained from these models can be used for developing appropriate closures for macroscopic models. The Eulerian–Eulerian approach is recommended for modeling of macro-scale flow processes in fixed bed as well as trickle bed reactors. The realistic representation of the characteristics of the fixed bed (porosity distribution, degree of anisotropy, and so on) is crucial for carrying out simulations for engineering applications. Most of the current work relies on empirical information and pressure drop data to calibrate computational flow models of fixed and trickle bed reactors. Such calibrated computational flow models will be useful for understanding issues related to maldistribution, channeling, formation of hotspots, etc. To realize process intensification and performance enhancement, accurate knowledge of the underlying flow field in chemical reactors is essential. The approach and computational models developed in this book will allow reactor engineer to harness the power of computational flow modeling for better reactor engineering.

Adequate attention to some of the key issues mentioned here and creative use of computational flow modeling will make significant contributions in enhancing engineering insight and engineering practice. Applications of various modeling aspects discussed so far to reactor performance evaluation and scale-up with some examples are discussed in the following two chapters.

REFERENCES

Al-Dahhan, M. H., & Dudukovic, M. P. (1994). Pressure drop and liquid holdup in high pressure trickle-bed reactors. *Chemical Engineering Science, 49*(24), 5681.

Al-Dahhan, M. H., Wu, Y., & Dudukovic, M. P. (1995). Reproducible technique for packing laboratory-scale trickle-bed reactors with a mixture of catalyst and fines. *Industrial and. Engineering Chemistry Research, 34*(3), 741–747.

Attou, A., & Ferschneider, G. A. (1999). Two-fluid model for flow regime transition in gas–liquid trickle-bed reactors. *Chemical Engineering Science, 54*(21), 5031.

Attou, A., & Ferschneider, G. (2000). A two-fluid hydrodynamic model for the transition between trickle and pulse flow in a cocurrent gas–liquid packed-bed reactor. *Chemical Engineering Science, 55*, 491.

Boelhouwer, J. G., Piepers, H. W., & Drinkenburg, A. A. H. (2002). Liquid-induced pulsing flow in trickle-bed reactors. *Chemical Engineering Science, 57*, 3387.

Calis, H. P. A., Nijenhuis, J., Paikert, B. C., Dautzenberg, F. M., & van den Bleek, C. M. (2001). CFD modelling and experimental validation of pressure drop and flow profile in a novel structured catalytic reactor packing. *Chemical Engineering Science, 56*, 1713.

Carman, P. C. (1937). Fluid flow through granular beds. *Trans. Inst. Chem. Eng., 15*, 150–166.

Crine, M., Marchot, P., & L'Homme, G. A. (1979). Mathematical modeling of the liquid trickling flow through a packed bed using the percolation theory. *Computers and Chemical Engineering, 3*, 515.

Davidson, M. R. (2000). Boundary integral prediction of the spreading of an inviscid drop impacting on a solid surface. *Chemical Engineering Science, 55*, 1159.

Davidson, M. R. (2002). Spreading of inviscid drop impacting on liquid film. *Chemical Engineering Science, 57*, 3639.

Dhole, S. D., Chhabra, R. P., & Eswaran, V. (2004). Power law fluid through beds of spheres at intermediate Reynolds numbers: pressure drop in fixed and distended beds. *Chemical Engineering Research and Design, 82*(A6), 1–11.

Dixon, A. G., & Nijemeisland, M. (2001). CFD as a design tool for fixed-bed reactors. *Industrial and Engineering Chemistry Research, 40*, 5246.

Dixon, A. G., Taskin, M. E., Nijemeisland, M., & Stit, E. H. (2008). Wall-to-particle heat transfer in steam reformer tubes: CFD comparison of catalyst particles. *Chemical Engineering Science, 63*(8), 2219–2224.

Donohue, T. J., & Wensrich, C. M. (2008). A numerical investigation of the void structure of fibrous materials. *Powder Technology, 186*(1), 72–79.

Durst, F., Haas, R., & Interthal, W. (1987). The nature of flows through porous media. *Journal of Non-Newtonian Fluid Mechanics, 22*, 169.

Ergun, S. (1952). Flow through packed columns. *Chemical Engineering Progress, 48*, 89–94.

Foumeny, E. A., & Benyahia, F. (1993). Can CFD improve the handling of air, gas and gas–liquid mixtures? *Chemical Engineering Progress, 91*(1), 8–9, 21.

Freund, H., Zeiser, T., Huber, F., Klemm, E., Brenner, G., Durst, F., et al. (2003). Numerical simulations of single phase reacting flows in randomly packed/fixed-bed reactors and experimental validation. *Chemical Engineering Science, 58*, 903.

Fukai, J., Shiiba, Y., Yamamoto, T., Miyatake, O., Poulikakos, D., Megaridis, C. M., et al. (1995). Wetting effects on the spreading of a liquid droplet colliding with a flat surface: experiment and modeling. *Physics of Fluids, 7*, 236.

Fukai, J., Zhao, Z., Poulikakos, D., Megaridis, C. M., & Miyatake, O. (1993). Modeling of the deformation of a liquid droplet impinging upon at surface. *Physics of Fluids A, 5*, 2588.

Grosser, K., Carbonell, R. G., & Sundaresan, S. (1988). Onset of pulsing in two-phase concurrent downflow through a packed bed. *AIChE Journal, 34*, 185.

Gunjal, P. R., & Ranade, V. V. (2007). Modeling of laboratory and commercial scale hydroprocessing reactors using CFD. *Chemical Engineering Science, 62*, 5512–5526.

Gunjal, P. R., Ranade, V. V., & Chaudhari, R. V. (2003). Liquid phase residence time distribution in trickle bed reactors: experiments and CFD simulations. *The Canadian Journal of Chemical Engineering, 81*, 821.

Gunjal, P. R., Kashid, M. N., Ranade, V. V., & Chaudhari, R. V. (2005). Hydrodynamics of trickle-bed reactors: experiments and CFD modeling. *Industrial and Engineering Chemistry Research, 44*, 6278–6294.

Gunjal, P. R., Chaudhari, R. V., & Ranade, V. V. (2005a). Computational study of a single-phase flow in packed beds of spheres. *AIChE Journal, 51*(2), 365–378.

Gunjal, P. R., Chaudhari, R. V., & Ranade, V. V. (2005b). Dynamics of drop impact on solid surface: experiments and VOF simulations. *AIChE Journal, 51*(1), 59–78.

Hill, R. J., Koch, D. L., & Ladd, A. J. C. (2001). Moderate-Reynolds-number flows in ordered and random arrays of spheres. *Journal of Fluid Mechanics, 448*, 243.

Hirt, C. W., & Nichols, B. D. (1981). Volume of fluid (VOF) method for the dynamics of free boundaries. *Journal of Computational Physics, 39*, 201.

Holub, R. A., Dudukovic, M. P., & Ramachandran, P. A. (1992). A phenomenological model for pressure drop, liquid holdup, and flow regime transition in gas–liquid trickle flow. *Chemical Engineering Science, 47*(9–11), 2343.

Holub, R. A., Dudukovic, M. P., & Ramachandran, P. A. (1993). Pressure drop, liquid hold-up and flow regime transition in trickle flow. *AIChE Journal, 39*, 302.

Irandoust, S., & Anderson, B. (1988). Monolithic catalysts for nonautomobile applications. *Catalysis Reviews: Science and Engineering, 30*(3), 341–392.

Jiang, Y. (2000). Flow Distribution and its Impact on Performance of Packed-Bed Reactors. *Ph.D. Thesis*. St. Louis, MO: Washington University.

Jiang, Y., Khadilkar, M. R., Al-Dahhan, M. H., & Dudukovic, M. P. (2000). Single phase flow modeling in packed beds: discrete cell approach revisited. *Chemical Engineering Science, 55*(10), 1829–1844.

Jiang, Y., Khadilkar, M. R., Al-Dahhan, M. H., & Dudukovic, M. P. (2001). CFD modeling of multiphase flow distribution in catalytic packed bed reactors: scale down issues. *Catalysis Today, 66*, 209–218.

Jiang, Y., Khadilkar, M. R., Al-Dahhan, M. H., & Dudukovic, M. P. (2002). CFD modeling of multiphase in packed bed reactors: results and applications. *AIChE Journal, 48*, 716.

Jongen, T. (1992). In: *Simulation and Modeling of Turbulent Incompressible Flows. PhD Thesis*. EPF Lausanne. Lausanne, Switzerland.

Kader, B. (1993). Temperature and concentration profiles in fully turbulent boundary layers. *International Journal of Heat Mass Transfer, 24*(9), 1541.

Kashiwa, B. A., Padial, N. T., Rauenzahn, R. M., & Vander-Heyden, W.B. (1994). A cell centered ICE method for multiphase flow simulations. In ASME symposium on numerical methods for multiphase flows. Lake Tahoe, NV.

Kim, S. E., & Choudhury, D. (1995). A near-wall treatment using wall functions sensitized to pressure gradient. In *ASME FED. Separated and complex flows, Vol. 217*. ASME.

Launder, B. E., & Spalding, D. B. (1974). The numerical calculations of turbulent flows. *Computational Methods of Applied Mechanical Engineering, 3*, 269.

Logtenberg, S. A., Nijemeisland, M., & Dixon, A. G. (1999). Computational fluid dynamics simulations of fluid flow and heat transfer at the wall–particle contact points in a fixed bed reactor. *Chemical Engineering Science, 54*, 2433.

Lopes, R. J. G., & Quinta-Ferreira, Rosa M. (2009). CFD modelling of multiphase flow distribution in trickle beds. *Chemical Engineering Journal, 147*, 342–355.

Magnico, P. (2003). Hydrodynamic and transport properties of packed bed in small tube-to-sphere diameter ratio: pore scale simulation using an Eulerian and a Lagrangian approach. *Chemical Engineering Science, 58*, 5005.

Maier, R. S., Kroll, D. M., Kutovsky, Y. E., Davis, H. T., & Bernard, R. S. (1998). Simulation of flow through bead packs using the lattice-Boltzmann method. *Physics of Fluids, 10*, 60.

Mantle, M. D., Sederman, A. J., & Gladden, L. F. (2001). Single and two-phase flow in fixed-bed reactors: MRI flow visualization and lattice-Boltzmann simulation. *Chemical Engineering Science, 56*, 523.

Martin, J. J., McCabe, W. L., & Monrad, C. C. (1951). Pressure drop through stacked spheres. *Chemical Engineering Progress, 47*(2), 91.

McHyman, J. (1984). Numerical methods for tracking interfaces. *Physica D: Non-linear Phenomena, 12*, 396–407.

Mehta, D., & Hawley, M. C. (1969). Wall effect in packed column. *Industrial and Engineering Chemistry Process Design and Development, 8*, 280–282.

Mewes, D., Loser, T., & Millies, M. (1999). Modelling of two-phase flow in packings and monoliths. *Chemical Engineering Science, 54*, 4729.

Monaghan, J. J. (1994). Simulating free surfaces with SPH. *Journal of Computational Physics, 110*, 339.

Mueller, G. E. (1991). Prediction of radial porosity distribution in randomly packed fixed beds of uniformly sized spheres in cylindrical containers. *Chemical Engineering Science, 46*, 706.

Natarajan, R., & Acrivos, A. (1993). The instability of the steady flow past spheres and disks. *Journal of Fluid Mechanics, 254*, 323.

Nemec, D., & Levec, J. (2005). Flow through packed bed reactors: 1. Single phase flow. *Chemical Engineering Science, 60*, 6947–6957.

Nijemeisland, M., & Dixon, A. G. (2001). Comparison of CFD simulations to experiment for convective heat transfer in a gas–solid fixed bed. *Chemical Engineering Journal, 82*, 231.

Nijemeisland, M., Dixon, A. G., & Stitt, H. (2004). Catalyst design by CFD for heat transfer and reaction in steam reforming. *Chemical Engineering Science, 59*, 5185–5191.

Ranade, V. V. (1994). Modelling of flow maldistribution in a *fixed bed* reactor using PHOENICS. *The Phoenics Journal of Computational Fluid Dynamics and it's Applications, 7*(3), 59–72.

Ranade, V. V. (1997). Improve reactor via CFD. *Chemical Engineer, 104*(May), 96–102.

Ranade, V. V. (2002). *Computational Flow Modeling for Chemical Reactor Engineering*. London: Academic Press.

Rao, V. G., Ananth, M. S., & Varma, Y. B. G. (1983). Hydrodynamics of two phase cocurrent downflow through packed beds. *AIChE Journal, 29*(3), 467.

Rider, W. J., & Kothe, D. B. (1995). Stretching and tearing interface tracking methods. *AIAA Paper*, 95–117, 171.

Rudman, M. (1997). Volume tracking methods for interfacial flow calculations. *International Journal for Numerical Methods in Fluids, 24*, 671.

Saez, A. E., & Carbonell, R. G. (1985). Hydrodynamic parameters for gas liquid cocurrent flow in packed beds. *AIChE Journal, 31*, 52.

Sangani, A. S., & Acrivos, A. (1982). Slow flow through a periodic array of spheres. *International Journal of Multiphase Flow, 8*, 343.

Sederman, A. J., & Gladden, L. F. (2001). Magnetic resonance visualization of single- and two-phase flow in porous media. *Magnetic Resonance Imaging, 19*, 339.

Sederman, A. J., Johns, M. L., Bramley, A. S., Alexander, P., & Gladden, L. F. (1997). Magnetic resonance imaging of liquid flow and pore structure within packed bed. *Chemical Engineering Science, 52*, 2239.

Seguin, D., Montillet, A., & Comiti, J. (1998). Experimental characterization of flow regimes in various porous media – I: limit of laminar flow regime. *Chemical Engineering Science, 53*(21), 3751.

Seguin, D., Montillet, A., Comiti, J., & Huet, F. (1998). Experimental characterization of flow regimes in various porous media – II: transition to turbulent regime. *Chemical Engineering Science, 53*(22), 3897.

SØrensen, J. P., & Stewart, W. E. (1974). Computation of forced convection in slow flow through ducts and packed beds − III. Heat and mass transfer in a simple cubic array of spheres. *Chemical Engineering Science, 29*, 827.

Specchia, V., & Baldi, G. (1977). Pressure drop and liquid hold up for two phase co-current flow in packed bed. *Chemical Engineering Science, 32*, 515.

Spedding, P. L., & Spencer, R. M. (1995). Simulation of packing density and liquid flow in fixed beds. *Computers and Chemical Engineering, 19*, 43.

Stephenson, J. L., & Stewart, W. E. (1986). Optical measurements of porosity and fluid motion in packed beds. *Chemical Engineering Science, 41*, 2161.

Suekane, T., Yokouchi, Y., & Hirai, S. (2003). Inertial flow structures in a simple-packed bed of spheres. *AIChE Journal, 49*, 1.

Szady, M. J., & Sundaresan, S. (1991). Effect of boundaries on trickle bed hydrodynamics. *AIChE Journal, 37*, 1237.

Thompson, K. E., & Fogler, H. S. (1997). Modeling flow in disordered packed beds from pore-scale fluid mechanics. *AIChE Journal, 43*(6), 1377.

Tobis, J. (2000). Influence of bed geometry in its frictional resistance under turbulent flow conditions. *Chemical Engineering Science, 55*, 5359.

Unverdi, S. O., & Tryggvason, G. (1992). A front tracking method for viscous, incompressible, multi-fluid flows. *Journal of Computational Physics, 100*, 25.

Van Hasselt, B. W., Lindenbergh, D. J., Calis, H. P., Sie, S. T., & Van Den Bleek, C. M. (1997). The three-levels-of-porosity reactor. A novel reactor for countercurrent trickle-flow processes, *Chemical Engineering Science, 52*(21−22), 3901−3907.

Wolfstein., M. (1969). The velocity and temperature distribution of one-dimensional flow with turbulence augmentation and pressure gradient. *International Journal of Heat and Mass Transfer, 12*, 301.

Yin, F. H., Sun, C. G., Afacan, A., Nandakumar, K., & Chung, K. T. (2000). CFD modeling of mass-transfer processes in randomly, packed distillation columns. *Industrial and Engineering Chemistry Research, 39*, 1369.

Zeiser, T., Steven, M., Freund, H., Lammers, P., Brenner, G., Durst, F., et al. (2002). Analysis of the flow field and pressure drop in fixed-bed reactors with the help of lattice Boltzmann simulations. *Philosophical Transactions of the Royal Society of London, Series A: Mathematical, Physical and Engineering Sciences, 360*, 507.